The Cryosphere Discuss., 8, 1723–1793, 2014
www.the-cryosphere-discuss.net/8/1723/2014/
doi:10.5194/tcd-8-1723-2014

The Cryosphere Discussions
Open Access

A 1-D model study of Arctic sea-ice salinity

P. J. Griewank and D. Notz

Max Planck Institute for Meteorology, Bundesstr. 53, 20146 Hamburg, Germany

Received: 31 January 2014 – Accepted: 27 February 2014 – Published: 26 March 2014

Correspondence to: P. J. Griewank (philipp.griewank@mpimet.mpg.de)

Published by Copernicus Publications on behalf of the European Geosciences Union.

Abstract

We use a 1-D model to study how salinity evolves in Arctic sea ice. To do so, we first explore how sea-ice surface melt and flooding can be incorporated into the 1-D thermodynamic SAMSIM sea-ice model presented by Griewank and Notz (2013). We introduce flooding and a flushing parametrization which treats sea ice as a hydraulic network of horizontal and vertical fluxes. Forcing SAMSIM with 36 years of ERA-interim atmospheric reanalysis data, we obtain a modeled Arctic sea-ice salinity that agrees well with ice-core measurements. The simulations hence allow us to identify the main drivers of the observed mean salinity profile in Arctic sea ice. Our results show a 1.5–4 $g\,kg^{-1}$ decrease of bulk salinity via gravity drainage after ice growth has ceased and before flushing sets in, which hinders approximating bulk salinity from ice thickness beyond the first growth season. In our simulations, salinity variability of first-year ice is mostly restricted to the top 20 cm. We find that ice thickness, thermal resistivity, freshwater column, and stored energy change by less than 5 % on average when the full salinity parametrization is replaced with a prescribed salinity profile. We conclude that for earth system models the impact of fully parametrizing the Arctic temporal salinity evolution is too small to justify the increase in computational cost and model complexity.

1 Introduction

Sea ice is a multi-phase material consisting of salty brine, fresh ice, and gas bubbles and is far from static. Brine moves through the ice and across the ice-ocean interface transporting dissolved tracers such as salt. The thermal properties of sea ice change along with the phase composition, bubbles form, dissolve, and escape into the atmosphere while chemical and biologic processes occur in the brine. Salt is a core component of sea ice as it along with temperature dictates the phase composition of sea ice through the liquidus relationship. It also influences the brine density, the chemical properties, the small scale sea-ice structure, and the vertical stratification of the underlying

TCD
8, 1723–1793, 2014

ocean via salt transport to the mixed layer. Unfortunately, the salinity of sea-ice is an elusive quantity which is difficult to observe. Many open questions related to the salinity evolution can not be answered due to the limited amount and the isolated nature of ice-core measurements, such as to what extent gravity drainage occurs during ice melt, what causes interannual salinity variability, how first-year ice transforms to multi-year ice, and how bulk salinity is linked to ice thickness. To fill these gaps in our understanding we here study the salinity evolution of Arctic sea ice and quantify the impact of the salinity evolution on various sea-ice properties using an expanded version of the Semi-Adaptive Multi-phase Sea-Ice Model (SAMSIM) introduced in Griewank and Notz (2013).

To do so, SAMSIM needed to be expanded to model sea-ice surface melt. The surface of melting sea ice is complex and highly heterogeneous. Melt water flows horizontally through snow and ice into melt ponds and cracks or percolates vertically through the ice. The properties of melting wet snow differ strongly from those of dry fresh snow, and the ice surface also deteriorates during melt and can form a layer of white deteriorated ice which is visually similar to snow (Eicken et al., 2002). All these processes influence albedo. Due to the large influence the ice albedo has on sea-ice evolution, the sea-ice modelling community has produced many albedo and melt pond parametrizations (e.g. Flocco and Feltham, 2007; Pedersen et al., 2009), but otherwise surface melt has received very little attention. All 1-D thermodynamic models since Maykut and Untersteiner (1971) have disregarded the physical structure and high gas fraction of the surface during melt, and treat melting sea ice as freshwater ice with modified thermal properties.

Over the last decade researchers have begun to parametrize the sea-ice salinity evolution (e.g. Vancoppenolle et al., 2006, 2007, 2009; Wells et al., 2011; Hunke et al., 2011; Rees Jones and Worster, 2013; Turner et al., 2013) to study the biogeochemical and physical processes in and below sea ice (e.g. Vancoppenolle et al., 2010; Tedesco et al., 2010, 2012; Jeffery et al., 2011; Saenz and Arrigo, 2012; Jardon et al., 2013). Despite these developments, the only published sea-ice model with a fully parameterized

TCD
8, 1723–1793, 2014

salinity evolution is the LIM 1-D model of Vancoppenolle et al. (2007) based on the 1-D thermodynamic model of Bitz and Lipscomb (1999). Accordingly, many possible approaches to model surface melt and parametrize salinity remain unexplored in 1-D sea-ice models. We introduce new schemes to parametrize surface melt, flooding, and flushing within our 1-D sea-ice model SAMSIM, making it capable of simulating the full growth and melt cycle of sea ice including the salinity evolution.

We force SAMSIM with Arctic reanalysis data to study the desalination processes and the resulting salinity evolution in the Arctic. This is the first general multi-year model study of sea-ice salinity throughout the Arctic. The only previous model study of sea-ice salinity is the study by Vancoppenolle et al. (2007) which focuses on two ice-core sites of land fast ice from 1999–2001. Model studies are necessary as measurement campaigns can only provide brief glimpses of the full salinity evolution, whereas we can easily explore a far greater diversity of conditions over a longer time frame. The simulated salinity profiles are compared to ice-core measurements to evaluate the model performance.

We have decided to limit the study to the Arctic because flooding and the corresponding snow ice formation play a large role in the Antarctic. As explained in detail in Sect. 2.4.4, we treat the flooding parametrizations currently implemented in SAMSIM as ad hoc solutions only suitable for dealing with isolated and sporadic flooding events. Accordingly, we will refrain from studying Antarctic ice until flooding is better understood.

The final topic we address is how parametrizing the salinity affects various sea-ice properties important to climate models. As sea-ice components of climate models are slowly becoming more sophisticated and modelers have begun to treat sea-ice salinity as a variable instead of a prescribed value or profile (e.g Vancoppenolle et al., 2009; Turner et al., 2013), it remains unclear how much model performance can be improved by fully parametrizing the temporal salinity evolution, and how sophisticated the parametrizations should be to balance the improvements against the increase in computational cost and code complexity.

TCD
8, 1723–1793, 2014

This paper is organized as follows. In Sect. 2 we detail how surface melt, flooding, and flushing are implemented in SAMSIM. The section ends with a description of the three separate salinity approaches used to parametrize salinity in SAMSIM and a discussion of the relative numerical costs associated with these approaches. In Sect. 3 we conduct an idealized melting experiment to study flushing and to determine how sensitive SAMSIM responds to changes of key parameters. In Sect. 4 we study the salinity evolution of 36 years of simulated sea ice forced with ERA-interim reanalysis data taken from throughout the Arctic. The simulations are split into first-year and multi-year ice which are analyzed separately and compared to ice-core data. The final Sect. 5 uses the same atmospheric forcing as Sect. 4 to quantify the impact of the various salinity approaches on quantities relevant to climate-models in order to evaluate if climate models would benefit from a fully parametrized temporal salinity evolution in their sea-ice sub models.

2 Model description

For the purpose of this paper, we expand the SAMSIM model which we first described in Griewank and Notz (2013). SAMSIM (Semi-Adaptive Multi-phase Sea-Ice Model) is a 1-D column model which employs a semi-adaptive grid. In this section we will introduce how SAMSIM treats surface ablation and processes related to surface melting as well as flooding.

We provide a very brief description of the fundamentals of SAMSIM in Sect. 2.1, a detailed description can be found in Griewank and Notz (2013). Following the brief description of SAMSIM we address a small modification of the gravity drainage parametrizations originally presented in Griewank and Notz (2013) in Sect. 2.2. Section 2.3 addresses how sea-ice melts in reality and in SAMSIM. The final additions to SAMSIM are the parametrizations of flushing and flooding introduced in Sect. 2.4. In Sect. 2.5 we describe the three salinity setups used in SAMSIM. Section 2.5 includes a discussion of the numerical costs and merits of each of the salinity approaches.

TCD
8, 1723–1793, 2014

2.1 SAMSIM

Each layer of SAMSIM is defined by the four fundamental variables mass m, absolute salinity S_{abs}, absolute enthalpy H_{abs}, and thickness Δz. Absolute values are simply the integral over the mass weighted bulk salinity S_{bu} and enthalpy H. The solid and liquid mass fractions ψ_s and ψ_l, as well as the solid, liquid, and gas volume fraction ϕ_s, ϕ_l, and ϕ_g are derived from the fundamental variables. A salt-free snow layer can exist on the ice, which has a variable density that affects the snow thermal conductivity. However, the only process currently implemented in SAMSIM which affects the snow density is rainfall into snow. In this paper, we refer to a specific layer by an upper right index counting from top to bottom, with the exception of the snow layer which is marked with "snow". E.g. m^6 is the mass of the sixth layer from the surface, m^1 is the mass of the top ice layer, and m^{snow} is the mass of the snow layer.

SAMSIM is the only sea-ice model to employ a semi-adaptive grid which grows and shrinks in discrete steps of Δz_0 at the ice-ocean interface (Griewank and Notz, 2013). However, at the ice-atmosphere boundary it is necessary to have a freely adjustable boundary to deal with incremental surface ablation and snow to ice conversion. This is addressed by letting the top ice layer thickness vary freely between $1/2\Delta z_0$ and $3/2\Delta z_0$. Once the top ice layer grows thicker than $3/2\Delta z_0$ it is split into two layers, the lower layer of the two with a thickness of Δz_0. Similarly when the top ice layer shrinks below $1/2\Delta z_0$ it is merged together with the second layer. A sketch of how a grid with three top ice layers evolves during melt is shown in Fig. 1.

The short wave radiation properties of the ice are set with a number of parameters which determine how much radiation is absorbed at the ice surface and how much of the radiation penetrates into the ice and is absorbed in the lower layers. These parameters are the albedo alb, the fraction of penetrating short wave radiation pen, and the optical thickness of the ice κ. Various parametrizations have been proposed which define the optical properties based on the surface temperature, ice thickness, and ablation rates. In SAMSIM the gas volume fraction could also be used to parametrize the

TCD
8, 1723–1793, 2014

optical properties, as the amount of air bubbles has a large impact on the optical properties of the ice (Light et al., 2008). However, because the focus of this paper is on the salinity evolution we will use constant values of alb, pen, and κ for sea ice to remove a source of variability in the model results (values shown in Table 1).

2.2 Modified gravity drainage

We have implemented a slight change to the calculation of the Rayleigh number of the layer i which is used in the gravity drainage parametrizations introduced in Griewank and Notz (2013) as

$$R^i = \frac{g\Delta\rho^i\tilde{\Pi}^i h^i}{\kappa\mu}.$$

The terms that enter the equation are the standard gravity g, the density difference between the brine in layer i and the lowest layer $\Delta\rho^i$, the distance from the layer i to the ocean h^i, the thermal diffusivity κ, the dynamic viscosity μ, and the permeability term $\tilde{\Pi}^i$. We have modified the Rayleigh number by replacing $\tilde{\Pi}^i$ with the bulk permeability $\overline{\Pi}^i$ for a Darcy through a stack of layers, which is given by the harmonic mean over all layers from i to the lowest layer n

$$\overline{\Pi}^i = \frac{\sum_{k=n}^{i}\Delta z^k}{\sum_{k=n}^{i}\frac{\Delta z^k}{\Pi^k}}.$$

Π^i is the permeability and Δz^i is the thickness of the layer i. In Griewank and Notz (2013) instead of the harmonic mean the minimal permeability $\tilde{\Pi}^i = \min(\Pi^i, \Pi^{i+1}, ..., \Pi^n)$ was used as a simplification. However, Vancoppenolle et al. (2013) demonstrated that using the minimal permeability instead of the harmonic mean leads to substantially different Rayleigh numbers. Accordingly, we replace the minimal permeability with the harmonic mean in the definition of the Rayleigh number.

TCD
8, 1723–1793, 2014

Changing the definition of the Rayleigh number requires the free parameters α and R_{crit} to be readjusted which link the amount of brine leaving each layer $\text{br}_{\downarrow}^{i}$ to the Rayleigh number, timestep $\text{d}t$, and layer thickness Δz via

$$\text{br}_{\downarrow}^{i} = \alpha(R^{i} - R_{\text{crit}})\Delta z^{i} \cdot \text{d}t.$$

To readjust α and R_{crit}, the same procedure is used which was used to initially determine the free parameters in Griewank and Notz (2013). The procedure numerically derives values which lead to the best agreement between modelled salinity and the laboratory measurements of Notz (2005). Two separate sets of measurements and the mean of the two sets are used, resulting in the following free parameter pairings: $\alpha = 0.000510, R_{\text{crit}} = 7.10$; $\alpha = 0.000681, R_{\text{crit}} = 3.23$; $\alpha = 0.000584, R_{\text{crit}} = 4.89$. As in Griewank and Notz (2013), we will use the values optimized to fit the mean of the two measurement sets as the default values, which are $\alpha = 0.000584, R_{\text{crit}} = 4.89$. In Sect. 4.3.3 the effect of the parameter uncertainty of α and R_{crit} on the multi-year salinity profile is addressed.

Updating the Rayleigh number definition has a substantial effect on the modelled salinity evolution of both the complex and simple gravity drainage parametrizations. However, the qualitative conclusions of Griewank and Notz (2013) and this paper are unaffected by the changed definition of the Rayleigh number. That the qualitative results are unaffected by the change in Rayleigh number definition can be seen by comparing this paper to the results of Griewank (2014), which uses the same simulations but the original Rayleigh number definition of Griewank and Notz (2013).

2.3 Surface melt

There are two main difficulties which complicate simulating surface melt in a 1-D thermodynamic sea-ice model. The first is the strong spatial heterogeneity of melting sea ice. Although certain aspects such as melt ponds can be parametrized, there is no way to overcome the fact that a 1-D approximation is less valid for melting sea ice than for

TCD
8, 1723–1793, 2014

growing sea ice. The second major difficulty is that many physical processes which occur at the surface during sea-ice melt are poorly understood. This is especially true for processes which occur at the snow-ice boundary and processes which involve capillary forces in snow or ice.

We have decided against separating the 1-D column into a ponded and non-ponded fraction, as this is impossible without sacrificing physical consistency in a number of ways. A possible compromise is to couple a 1-D column with a melt pond cover to another 1-D column with no pond. A melt pond and albedo parametrization could be introduced to modify short-wave radiation penetration and reflectance without any effect on sea-ice permeability, freeboard, or melt water formation. However, we have decided to not introduce such an albedo parametrization for two reasons. Firstly, most albedo parametrizations are not suitable for SAMSIM. For example, some parametrizations change the albedo as an empirical function of surface temperature. If the parametrization assumes that the surface layer is salt free, the parametrization will assume that the surface temperature during melt will always be at 0 °C. However in SAMSIM, the surface temperature varies during melt depending on the salinity of the top ice layer. Other parametrizations rely on the surface melt speed, which is not a variable in SAMSIM. Instead SAMSIM has melt water formation and surface ablation, which are linked but not identical. The second reason is that slight albedo changes would overshadow the effects of the sea-ice salinity. If the albedo parametrization were fully physically consistent with SAMSIM this would be acceptable. However, albedo parametrizations mostly rely on empirical measurements and are intended to improve large-scale models and are ill-suited to determine how the albedo would react to a 5 % increase of gas volume fraction or a 0.1 °C increase of temperature in the top ice layer of SAMSIM. Including an albedo parametrization would result in a high non-physical source of variability which would greatly complicate interpreting the results. Extending SAMSIM by an albedo parametrization that is compatible with SAMSIM physics remains, however, desirable and will be subject to future work. For now, we simply use a constant value for the ice albedo.

TCD
8, 1723–1793, 2014

From the measurements taken at the Surface Heat Budget of the Arctic Ocean Project (SHEBA) site, Eicken et al. (2002) identified three stages of melt for Arctic multi-year ice. During stage I melt ponds form, fed by horizontal transport of melting snow. The snow cover still persists and while most of the melt water movement is horizontal, some melt water drains to the bottom of the ice through cracks and flaws in the ice. Stage II begins when the snow cover has completely melted away. During stage II melt water moves horizontally until it reaches flaws as well as vertically through the ice. In stage III the flaws have enlarged to the point of ice disintegration. Melt water moves vertically through the ice as well as horizontally until it reaches cracks and the edge of the ice flows, and convective overturning occurs close to the ice-ocean interface.

In SAMSIM, surface melt is implemented by separating melt into two separate stages. The first stage is snow melt, in which snow is converted to slush. This process thins the snow layer by transforming a fraction of the snow into slush, which is then added to the top sea ice layer as described in Sect. 2.3.1. The second stage is surface ablation in which a fraction of the liquid volume of the top ice layer is designated as melt water as described in Sect. 2.3.2. This melt water is either transported directly into the ocean, or flows through the ice and cracks according to the flushing parametrization introduced in Sect. 2.4.2.

2.3.1 Snow melt

The physics of snow is very complex and a scientific field of its own. The snow layer in SAMSIM is intended to simulate only the most basic aspects of snow on sea ice. In contrast to the widely used 1-D thermodynamic sea-ice model of Bitz and Lipscomb (1999) which is implemented in both the Los Alamos (CICE) and the Louvain-la-Neuve (LIM) sea-ice models, snow does not turn directly into melt water in SAMSIM. Instead, melted snow from the snow surface percolates downward and accumulates on the sea-ice surface forming a slush layer of depth B as illustrated in Fig. 2. This snow to slush conversion in SAMSIM is based on two core assumptions. The first assumption is that the snow can only retain a maximum liquid mass fraction ($\psi_{\mathrm{l,max}}$) which is a function of

TCD
8, 1723–1793, 2014

the snow solid mass fraction. The function we use is

$$\psi_{\mathrm{l,max}} = 0.057 \frac{(1 - \psi_{\mathrm{s}}^{\mathrm{snow}})}{\psi_{\mathrm{s}}^{\mathrm{snow}}} + 0.017,$$

which we take from the laboratory study of Coleou and Lesaffre (1998). In Fig. 2 the volume fractions are shown instead of the mass fractions, because the volume fractions are proportional to the area depicted. The second core assumption is that when the liquid water content surpasses the retainable amount, the excess water pools at the bottom of the snow layer forming a layer of slush. At each time step the depth of the slush layer is determined and then the slush layer is added to the top ice layer.

Two additional assumptions are required to determine the slush depth which is marked as B in Fig. 2, namely the gas fraction of the slush $\phi_{\mathrm{g,melt}}$, and the solid fraction of the slush layer and remaining snow layer. We assume that the solid volume fraction equals the solid fraction of the previous time step, and that $\phi_{\mathrm{g,melt}}$ is a constant. In this paper we set $\phi_{\mathrm{g,melt}}$ to 20 %, which we base on the measured surface sea-ice densities of Eicken et al. (1995).

Following these assumptions, when the liquid volume fraction of the snow layer exceeds $\phi_{\mathrm{l,max}}$ the slush depth B is calculated from the snow solid fraction of the last time step ($\phi_{\mathrm{s}}^{\mathrm{snow}}$) and the gas content as

$$B = \Delta z \frac{\phi_{\mathrm{l}}^{\mathrm{snow}} - \phi_{\mathrm{l,max}}}{1 - \phi_{\mathrm{l,max}} - \phi_{\mathrm{s}}^{\mathrm{snow}} - \phi_{\mathrm{g,melt}}}.$$

As a result the top ice layer grows thicker by B, and mass and enthalpy are transfered according to the composition of the slush layer. To maintain the solid fraction of the last time step the snow needs to be compacted by A as illustrated in Fig. 2. In total the snow to slush conversion shrinks the snow layer by $A + B$, the total snow and ice column shrinks by A, and the top ice layer grows by B.

To our current knowledge, the approach of converting snow into slush before it can run off as melt water is unique. Compared to the standard approach in which melted

TCD
8, 1723–1793, 2014

snow is directly removed as melt water, our approach leads to a slight delay in the onset of flushing. In reality sea-ice has a varying surface height, which causes the melt water in the slush to flow into melt ponds. In SAMSIM, by the time the snow layer has melted away, the top model layers which were formed by snow to slush conversion are predominantly liquid and salt free but also contain the solid fraction of the melt water soaked snow. These top ice layers can be interpreted as a spatial average over melt ponds and snow remnants. As a result the snow melt stage of SAMSIM is shorter than the first melt stage of Eicken et al. (2002). Although the implemented snow to slush conversion neglects many of the finer aspects of snow physics, we trust that it captures snow melt more realistically than the standard approach of turning snow directly into melt water.

Two additional processes also convert snow to slush, flooding as introduced in Sect. 2.4.4 and melt water wicking. Wicking occurs when the top ice layer is so liquid that excess brine seeps into the snow. This process is incorporated into the model as introduced in the following subsection.

2.3.2 Surface ablation

Surface ablation begins once the snow layer has been completely transformed to slush and the top sea-ice layer is in direct contact with the atmosphere. Surface ablation in SAMSIM requires deciding how much of the liquid fraction runs off as melt water and how much of the departing melt water is replaced by gas. In reality the ice surface varies immensely in space and time, from dark deep melt ponds to deteriorated white ice which looks like snow from afar (Eicken et al., 2002). In contrast, the ice surface in SAMSIM is solely represented by the phase composition of the top ice layer.

The way we define melt water is that melt water is the fraction of the brine in the top ice layer which can leave the top layer. Melt water can leave the top layer via flushing which causes surface ablation, or by wicking into the snow layer as explained at the end of Sect. 2.3.1. In the model melt water has the same temperature and brine salinity

TCD
8, 1723–1793, 2014

as the brine in the top layer. At each time step the amount of melt water is calculated independently of the previous amount of melt water.

Melt water formation and runoff in SAMSIM is restricted to the top ice layer and is based on three assumptions. The first is that ice melted at the ice surface directly turns into melt water. The second is that if the solid fraction of the top ice layer sinks below a minimal low value, excess brine is free to flow off as melt water. The third is that over time the gas fraction increases until it reaches the value of $\phi_{\mathrm{g,\,melt}}$.

Melt water can form by surface melting as soon as the surface temperature surpasses the freezing temperature given by the bulk salinity of the top ice layer. The amount of melt water formed is determined by the amount of latent heat release necessary to balance the energy difference between the atmospheric heat flux to the surface and the flux from the surface into the top ice layer (depicted in Fig. 3). This approach is commonly used in sea-ice thermodynamic models (e.g. Bitz and Lipscomb, 1999) but needs to be adapted to incorporate the varying density and gas fraction of SAMSIM. The discretized diffusive heat flux from the ice surface into the top ice layer is

$$q^1 = -k^1 2 \frac{T^{\mathrm{freeze}} - T^1}{\Delta z^1}.$$

The thermal conductivity of the top ice layer k^1 is a linear combination of the liquid and solid phases, while the gas phase is treated as an insulator. The depth of the melt water film for a given atmospheric energy flux q^{atmos} is then

$$\Delta z_{\mathrm{melt}} = \frac{|q^{\mathrm{atmos}} - q^1|}{\phi_{\mathrm{s}}^1 \rho_{\mathrm{s}} L}.$$

The second way melt water can form is when the solid fraction of the top ice layer ϕ_{s}^1 falls below a minimal low value $\phi_{\mathrm{s,\,melt}}$. When this occurs the solid fraction is compacted by Δz_{melt} until the solid fraction reaches $\phi_{\mathrm{s,\,melt}}$ as shown in Fig. 4. From volume

TCD
8, 1723–1793, 2014

conservation it follows that

$$\Delta z_{\text{melt}} = \Delta z^1 \left(1 - \frac{\phi_s^1}{\phi_{s,\,\text{melt}}}\right).$$

This simplification ensures that melt water forms before the top ice layer is fully liquid. Not shown in the figure is that a similar limit exists on the gas fraction. If the gas fraction exceeds $\phi_{g,\,\text{melt}}$ then the top ice layer is compacted to reduce ϕ_g^1 to $\phi_{g,\,\text{melt}}$. $\phi_{g,\,\text{melt}}$ is the same parameter which determines the amount of air captured in the slush during snow melt, and is set to 0.2 based on density measurements at the surface of Eicken et al. (1995). To our knowledge there are no measurements from which to estimate $\phi_{s,\,\text{melt}}$. A range of values will be explored later in this paper, but as a first guess we assume a value of 0.4, which is slightly above the solid fraction assigned to fresh snow in SAMSIM. If the ice melts primarily through compacting due to low solid fractions, the top ice layer will approach the given values of $\phi_{g,\,\text{melt}}$ and $\phi_{s,\,\text{melt}}$ over time.

If the melt water forms due to a low solid fraction while snow is present, the melt water is assumed to wick up into the snow and creates a slush layer which is then added to the top ice layer again. We refer to this as wicking which is similar to snow melt (Fig. 2), except that the amount of water available to form slush is given by the amount of melt water present in the top ice layer.

2.4 Salinity parametrizations

There are three known relevant desalination processes in sea ice: gravity drainage, flushing, and flooding (Notz and Worster, 2009). We addressed how gravity drainage is implemented into SAMSIM in our previous publication (Griewank and Notz, 2013). In this subsection we introduce parametrizations for flushing and flooding, making SAMSIM the second published 1-D model capable of capturing the full salinity evolution. The first model capable of capturing the full salinity cycle is the 1-D LIM sea-ice model of Vancoppenolle et al. (2006).

TCD
8, 1723–1793, 2014

Parametrizing flushing faces the same challenges that modeling surface melting faces, namely high horizontal heterogeneity, insufficient data, and a lack of theoretical understanding. No quantitative laboratory studies of flushing have been published to this date, and due to sampling issues and challenging conditions field studies have been limited to studies of dye dispersion and ice-core salinity (Eicken et al., 2002). The understanding of flooding is even poorer, and is limited to the analysis of ice cores which contain flooded snow-ice.

2.4.1 Flushing

The first and only published flushing parametrization incorporated in a full thermodynamic sea-ice model by Vancoppenolle et al. (2006) assumes that once the ice reaches a certain permeability, a fraction of the melt water flows downward through the sea ice and into the ocean below. Although this approach neglects many aspects of flushing, it is able to reproduce field measurements of salinity (Vancoppenolle et al., 2007). In this subsection we will introduce two parametrizations. The complex parametrization attempts to model flushing as a physically consistent hydraulic system, and the simple parametrization is a numerically cheap alternative based on the assumption that the liquid fraction increases towards the surface during surface melt.

2.4.2 Complex flushing

It is known from the field observations of Eicken et al. (2002) that much of the brine movement during flushing occurs horizontally in the upper layers. Once the horizontally flowing melt water reaches a flaw or crack it drains below the sea-ice which can lead to underwater ice formation (Eicken et al., 1995; Notz et al., 2003). The parametrization of Vancoppenolle et al. (2006) has no explicit treatment of horizontal fluxes. Our goal is to design a flushing parametrization which is as physically consistent as possible in a 1-D model and includes horizontal brine fluxes which are highest close to the ice surface. Additionally the parametrization should have as few free parameters as possible. The

TCD
8, 1723–1793, 2014

resulting parametrization (sketched in Fig. 5) treats sea ice as a hydraulic network in which each model layer has a vertical and horizontal hydraulic resistance (R_v and R_h). The assumptions on which the parametrization is based are:

1. Cracks always exist in the ice, and the average horizontal distance between these flaws grows linearly with ice thickness.
2. Once brine reaches such a crack it drains away to the ice-ocean interface without interacting with the underlying ice layers.
3. The vertical resistance represents the resistance to brine flowing from the top to the bottom of a layer. The horizontal resistance represents the resistance which brine needs to overcome to reach a crack.
4. Flushing melt water flows vertically from layer to layer and horizontally to the cracks. The specific amount for each layer is determined by the hydraulic resistances and the hydraulic head.
5. The hydraulic head is assumed to be equal to the freeboard ζ, resulting in a pressure difference of $\Delta p = \zeta \rho g$ for the brine density ρ and gravitational constant g.

The resulting parametrization has only a single free parameter β which determines the average distance x to the next crack for a given ice thickness h through $x = \beta \cdot h$.

The Darcy flow in a porous medium with a hydraulic resistance of R leads to a mass flux f of

$$f = \frac{\Delta p \cdot A}{R} \rho$$

for the pressure difference Δp and liquid density ρ. In SAMSIM, for each layer i the vertical hydraulic resistance

$$R_v^i = \frac{\mu}{\Pi(\phi_l^i) A} \Delta z^i$$

TCD
8, 1723–1793, 2014

is defined by the permeability Π which is a function of the layer's liquid fraction ϕ_l^i, the brine viscosity μ, the column area A, and the layer thickness Δz.

To define the horizontal hydraulic resistance we take the average distance to the next crack from our assumptions resulting in

$$R_h^i = \frac{\mu}{\Pi(\phi_l^i) A_v^i} x.$$

In contrast to the vertical flow area A which is always $1\,m^2$ in the column model, the horizontal flow area A_v^i varies with layer thickness as well as with the geometry of the cracks and resulting flow field. We take A_v^i to be equal to the vertical layer surface with an area of $\Delta z^i \cdot 1\,m$.

The resulting horizontal and vertical brine fluxes ($\boldsymbol{f}_h$ and $\boldsymbol{f}_v$ as shown in Fig. 5) are then computed from hydraulic head and resistance. The total resistance over multiple layers is calculated as a sum of parallel and serial resistances, the same method used in resistor ladder circuits. The total flux is limited by the amount of melt water present in the top ice layer.

Vertical fluxes advect salt and heat from layer to layer using the upstream method, while horizontal fluxes transport both salt and heat directly to the lowest model layer, i.e. the ice-ocean interface. As the thermal profile in melting ice is almost uniform, the vertical fluxes lead to a smaller desalination than the horizontal fluxes.

Although the top ice layer can accumulate melt water faster than it can flush away, a fully liquid layer is impossible. As the top ice layer becomes more and more liquid, the permeability increases and the horizontal hydraulic resistance of the top ice layer decreases, resulting in a strong horizontal flushing in the top ice layer.

2.4.3 Simple flushing

We propose a second numerically cheaper parametrization which we will refer to as the simple flushing parametrization. In contrast to the complex parametrization which

TCD
8, 1723–1793, 2014

calculates brine fluxes which affect salinity via advection, the simple parametrization directly modifies the salinity to fulfill a stability criterion. This stability criterion is based on the simple assumption that the liquid fraction is highest in the top ice layer during melt, and decreases into the ice.

The implementation is as follows. At each time step the melt water which forms in the top ice layer as explained in Sect. 2.3.2 is removed. As the salinity of the melt water given by the ice-brine liquidus relationship is higher than the bulk salinity of the top ice layer, the melt water removal desalinates the top ice layer. At each time step it is checked if $\phi_l^1 > \phi_l^2$. Given that the temperature differences between the top layers is small during surface melt, the second saltier layer gradually becomes more liquid than the fresher top layer. When this occurs, the salinity of the second layer is simply reduced by a fixed fraction ϵ. The same procedure is then applied the next lower layer as long as $\phi_l^i > \phi_l^{i+1}$. For example if $\phi_l^1 < \phi_l^2 < \phi_l^3 > \phi_l^4 < \phi_l^5$, the salinity of the second and third layer are reduced.

2.4.4 Flooding

Flooding can occur when snow pushes the ice below the ocean surface, causing ocean water to well up and flood the snow. The resulting frozen mix of snow and ocean water called snow ice can be identified by various means in ice cores, from which we know that flooding occurs mainly in the Antarctic and contributes up to 25 % of ice production in certain areas (Jeffries et al., 2001; Maksym and Jeffries, 2001). We base our understanding and treatment of flooding on the work of Ted Maksym and Martin O. Jeffries (Maksym and Jeffries, 2000, 2001; Jeffries et al., 2001). To readers interested in flooding we recommend the PhD thesis by Maksym (2001).

Although at first glance flooding seems to be the same process as flushing but with a reversed pressure gradient, there are a number of additional uncertainties. Field measurements have shown that a negative freeboard does not automatically lead to flooding, although the chance of flooding is higher the lower the freeboard. Additionally, very little is known about what happens to the flooded brine once it reaches the ice

TCD
8, 1723–1793, 2014

surface. As flooding occurs at the bottom of the snow mantel, direct observations of flooding are extremely difficult to obtain. Snow metamorphism is by itself a complex process, but the interactions between flooding brine and snow are even more complex and little research has been devoted to this specific issue. Brine movement must occur at the ice surface after or during flooding, because otherwise snow-ice salinities would be higher than the measured values.

As for flushing and gravity drainage we again developed two separate parametrizations for flooding. However, the two flooding parametrizations are rather similar. We will simply refer to the slightly more sophisticated parametrization as the complex parametrization and the simpler one as the simple flooding parametrization.

2.4.5 Complex flooding

The complex parametrization assumes that during flooding ocean water passes through cracks and channels in the ice to flood the snow layer. The flooding ocean water is assumed not to interact with the brine in the sea ice, as Maksym and Jeffries (2001) showed that if flooding resulted in an upward brine displacement through the whole ice the resulting desalination would quickly turn the ice impermeable. The flux of ocean water to the surface is calculated as a Darcy flow driven by the negative freeboard and limited by the permeability of the least permeable model layer. This approach can lead to a large negative freeboard if the ice layer is impermeable. To avoid this a maximum negative freeboard $\zeta_{\max}$ is defined. If the freeboard sinks below this threshold, the flux of ocean water necessary to raise the freeboard to the threshold is determined and applied.

The ocean water which is transported to the ice surface forms a slush layer which is added to the top ice layer. This is the same approach SAMSIM uses to imitate snow melt and melt water wicking into the snow layer (described in Sects. 2.3.1 and 2.3.2). However, given a snow solid volume fraction of approximately 30–40 % this approach would result in the flooded slush layer having a very high salinity of roughly 20 g kg^{-1}, which is inconsistent with measurements. To avoid this high salinity, we assume that

TCD
8, 1723–1793, 2014

the ocean water which floods the snow simultaneously wicks upward and dissolves additional snow into the slush which leads to a freshening of the slush. The ratio of dissolved to flooded snow is assumed to be constant, and is defined by an additional free parameter δ.

In this paper we use a value of 5 cm for ζ_{max}, which is based on the freeboard measurements analyzed in Maksym and Jeffries (2000) and for δ we use a value of 0.5 as a preliminary best guess.

2.4.6 Simple flooding

The simple parametrization is simply the complex parametrization stripped of the permeability dependent flooding speed and without snow dissolving into the slush layer. The simple parametrization is identical to the complex parametrization if the free parameters are set accordingly, $\zeta_{max} = 0$ m and $\delta = 0$. This means that as soon as a negative freeboard develops flooding sets in right away, and that no snow is dissolved into the forming slush.

2.5 Salinity setups

In Sect. 2.4 we have presented four parametrizations, two for flushing and two for flooding. Together with the two gravity drainage parametrizations introduced in Griewank and Notz (2013) SAMSIM now has two complete sets of desalination processes. The first set consists of the complex flushing, the complex flooding, and the complex gravity drainage parametrization. The second set of parametrizations consists of the simple flushing, the simple flooding, and the simple gravity drainage parametrization. The parametrizations of the first set all compute brine fluxes which result in salt and heat advection. Accordingly, the rate of salinity change is determined by the strength of brine flow and the salinity gradients between layers. In contrast, the parametrizations of the second set directly adjust the salinity profile to fulfill defined stability criteria.

TCD
8, 1723–1793, 2014

We will refer to the first set of parametrizations as the complex salinity approach, as it consists of the more sophisticated parametrizations which were designed to be as close to reality as possible. The second set will be referred to as the simple approach, as the parametrizations included were developed as simpler alternatives to the parametrizations of the complex approach.

The third and final salinity approach employed in this paper is to prescribe a depth dependent salinity profile which is completely independent of the ice properties. The profile used is the same introduced in Griewank and Notz (2013). The profile consists of a linear decrease in bulk salinity from 34 $g\,kg^{-1}$ at the ice-ocean interface to 4 $g\,kg^{-1}$ 15 cm above the bottom, and a second linear decrease from the 4 $g\,kg^{-1}$ 15 cm above the ice-ocean interface to 0 $g\,kg^{-1}$ at the surface. This approach is referred to as the prescribed approach. The prescribed profile is by choice highly idealized. A more realistic profile could have been derived from simulations using the complex approach, but we prefer the idealized profile as it is independent of both SAMSIM and the chosen forcing.

An important aspect of the complex parametrisation set is that the simulated brine fluxes result in heat fluxes both in the ice and into the ocean. This is most relevant during growth when gravity drainage continually moves colder brine to the ocean while taking up relatively warm ocean water, resulting in a small but steady increase of oceanic heat flux in our limited model domain. Because flushing mostly occurs in ice close to the freezing temperature the energy lost due to flushing is small. To keep the results of the three salinity approaches as comparable as possible, the heat fluxes resulting from gravity drainage and flushing are subtracted from the lowest layer at each time step. This heat flux modification was already applied in Griewank and Notz (2013).

Numerically, the complex approach is much more expensive than the simple approach because the brine dynamics and resulting salt advection require a much smaller time step at the same spatial resolution. If the amount of brine flowing into a layer is close to the liquid volume of the layer sudden salinity changes can lead to layers becoming impermeable and choking off all further flow. As the brine flows and the brine

TCD
8, 1723–1793, 2014

volume in the layers are continuously changing, there is no way to predict beforehand what time step will be needed for a specific experiment.

In comparison to the prescribed approach, the simple approach is not much more expensive in the 1-D model for the same amount of layers. However, because the simple approach is dependent on the vertical structure of the ice column its quality degrades if very few layers are used. Also, while the prescribed approach only depends on the total ice thickness, the simple approach also depends on the amount of salt in each layer. This is not of great importance in 1-D models, but if implemented in a model with horizontal ice advection the amount of tracers which need to be advected would lead to an increase of computational demands. In summary, the computational advantage of the prescribed approach over the simple approach is that the number of layers can be smaller and it requires no tracer advection, while the computational advantage of the simple approach over the complex approach is the ability to use longer time steps.

To provide a frame of reference, the very basic sea-ice component of the Max Planck Institute Ocean Model (MPIOM) consumes roughly 10–15 % of the total cost while the much more complex and not yet optimized LIM3 model is responsible for approximately 30 % of the total NEMO-LIM3 ice-ocean model. The two most computationally expensive components of sea-ice models are the dynamics and tracer advection. Sea-ice complicates the parallelization of ocean models, as an ice-covered ocean domain takes longer to compute than an ice-free domain, and the ice-covered domain can act as a bottle neck. If this is not taken into account and ice dynamics are not parallelized, the sea-ice component can slow down a coupled ice-ocean model by a factor of two.

Another cost of implementing additional processes and parametrizations into climate models is an increase of code complexity. Increasing code complexity reduces the understandability, flexibility, and maintainability of programs. These properties are all of great importance to climate models as these are normally developed, modified, maintained, and run by many scientists over decades. When deciding if and how to parametrize sea-ice salinity in a climate model the increase of computational cost and

TCD
8, 1723–1793, 2014

code complexity should be kept in mind. We discuss the trade off of increased precision vs. computational cost and model complexity in the final conclusions of this paper.

3 Idealized flushing experiments

In this section we take a closer look at the complex flushing parametrization and how sensitively it reacts to various parameters. To do so, we use a highly idealized experiment which aims to remove all feedbacks and processes other than flushing. As a full exploration of possible initial and boundary conditions and the parameter space would be a very expensive exercise, we limit ourselves to a single experimental setup and three parameters. For each of the three parameters the experimental setup is run repeatedly for a range of values, while the two other parameters remain fixed. The first parameter we vary is the minimum amount of solid fraction $\phi_{\mathrm{s,\,melt}}$ which can be present in the top ice layer before melt water forms. $\phi_{\mathrm{s,\,melt}}$ affects how permeable the top ice layer is when melt water forms. The second parameter we vary is β which determines the linear relationship of average horizontal flow distance to ice thickness. The third parameter is the layer thickness Δz_0. For the idealized experiment we set the total number of layers high enough so that all layers have the uniform thickness of Δz_0.

The idealized experiment begins with a two meter thick homogeneous slab of ice with a bulk salinity of $5\,\mathrm{g\,kg^{-1}}$ and a temperature of roughly $-1.3\,^{\circ}\mathrm{C}$. A constant oceanic heat flux of $15\,\mathrm{W\,m^{-2}}$ is applied to the bottom while a constant heat influx of $380\,\mathrm{W\,m^{-2}}$ is applied to the surface. After subtracting the outgoing thermal radiation at $0\,^{\circ}\mathrm{C}$ at the surface, the net heat input into the surface is slightly below $70\,\mathrm{W\,m^{-2}}$. All brine fluxes which occur in the experiment are caused by flushing as gravity drainage is deactivated and no flooding occurs. The setup of the idealized experiment was chosen to produce a strong flushing signature with chosen values not too far away from field conditions.

We will first make some general observation of how flushing occurs in the idealized experiment in Sect. 3.1 before analysing how sensitively the flushing parametrization reacts to the three parameters in Sects. 3.2, 3.3 and 3.4.

TCD
8, 1723–1793, 2014

3.1 General observations

In the idealized experiment the homogeneous sea-ice slab melts away over two months (Fig. 6). The constant surface heat input should lead to a constant rate of surface ablation, however SAMSIM's semi-adaptive grid results in a step wise surface ablation, especially at lower resolution (see Fig. 7d). As described in Sect. 3, the fresh melt water which drains through flaws and cracks can accumulate beneath the ice in the lowest model layer. This effect is visible in the temperature plot of Fig. 7, where a thin line of orange at the ice-ocean boundary shows accumulated melt water.

One of two striking features of this idealized experiment is that while flushing reduces the bulk salinity close to the surface it also leads to a high increase of salinity at the bottom (Figs. 6, 7b–d, and 8). This is caused by the positive temperature gradient near the ice-ocean interface, which leads to the vertically flushing brine to move from colder to warmer layers. As the brine is saltier in the colder layers due to the liquidus relationship, salt advection leads to a bulk salinity increase in the lowest ice layers. This effect disappears if gravity drainage is activated (Fig. 7a), which explains why this salinity increase due to flushing has not been observed to our knowledge. To determine if flushing could in principle lead to such an increase in salinity if gravity drainage is absent would require experiments with a multi-phase material in which both phases have a similar density to inhibit convection. An additional requirement needed to generate these high salinities close to the ice-ocean interface is that the oceanic heat flux is relatively small so that the salt has time to accumulate in the lower layers before they melt away. The low oceanic heat flux also allows melt water to accumulate in the very lowest layer where melt water is transported by flushing (Fig. 7b and c).

The second most striking feature is that the desalination near the surface occurs in waves, which can be seen by following the $3\,\mathrm{g\,kg^{-1}}$ contour in Figs. 6 and 7. As the rate of melt water formation is nearly constant over time, this oscillation shows that the ratio of horizontal to vertical flushing oscillates over time. The speed, form, and strength of these oscillations are dependent on the chosen values of ϕ_s^{top}, β, and Δz_0, which

TCD
8, 1723–1793, 2014

indicates that the complex flushing parametrization does not reach an equilibrium and is dependent on model parameters (Fig. 7b–d). The oscillation is also visible when comparing the salinity profiles of the experiment at 30 and 34 days (Fig. 8). At 30 days there is almost no visible difference between $\beta = 1$, 5, and 25. Four days later a smooth progression is visible. Similarly, the grid spacings 4, 8, and 16 mm are almost identical at 34 days, but at 30 days this is not the case. Such an oscillatory behavior is physically plausible. At the beginning of the experiment flushing penetrates deep into the still saline ice and desalinates the upper layers. The desalination leads to an increase of the solid fraction and a slight warming. The underlying layers which have not yet been desalinated remain cooler. At some point the lowest desalinated layer is cooled enough by the lower layers so that the liquid reduces enough to make the ice impermeable. The now impermeable layer shields the lower layers from vertical flushing and the melt water flows horizontally into cracks and flaws. Over time the surface melts away until the impermeable layer which shielded the lower layers reaches the surface. Once the fresh layer is melted away, flushing melt water penetrates deep into the ice desalinating the upper layers, and the cycle repeats itself.

Local short-term flushing events have been detected in the temperature profiles of both field data (Pringle et al., 2007) and laboratory experiments (Wiese, 2012). However, averaging horizontally over a large area should average out the local flushing events to a gradual and smooth desalination. Accordingly, to get a representative salinity profile from SAMSIM it is best to perform a short temporal average over one or two oscillations.

3.2 Minimal surface solid fraction

The minimal surface solid fraction defines how low the solid fraction of the top ice layer can sink before melt water is formed as described in Sect. 2.3.2. The range of possible values of $\phi_{\mathrm{s,melt}}$ is constrained by physical and model limitations to be between 0 and $1 - \phi_{\mathrm{g,melt}}$. We choose to vary $\phi_{\mathrm{s,melt}}$ between 0.2 and 0.5, which we trust to span the range of realistic values with a default value of 0.4. The effect of $\phi_{\mathrm{s,melt}}$ on the complex

TCD
8, 1723–1793, 2014

flushing parametrization seems to be rather small, with only slight differences visible in the resulting salinity profiles (Fig. 8a and b). In the idealized experiment, lower values of $\phi_{s,\,melt}$ cause slightly stronger salinity changes in the idealized experiment (Fig. 6b vs. Figs. 7b and 8a and b). As $\phi_{s,\,melt}$ also affects snow to slush transformation, it is possible that the effect of $\phi_{s,\,melt}$ is stronger when snow is present.

3.3 Free parameter β

In contrast to $\phi_{s,\,melt}$ we have no definitive physical or model limits on the possible value of β. Based on tracer studies of Eicken et al. (2002), we expect horizontal flows to be on the order of meters. Accordingly, we expect β to be in the single digits. However, to account for unknown biases in the model and parametrization (e.g. permeability) we chose a very wide spread of values from 0.04 to 25 to err on the side of caution. As a working assumption we use 1 as the default value.

As a high β increases the horizontal hydraulic resistance, the higher β is the weaker the horizontal fluxes are and vice versa. In the idealized experiment the low value of $\beta = 0.04$ leads to the flushing brine only penetrating a short distance into the ice (Fig. 8 c and d). Higher values of β cause an increased salinity at the ice-ocean interface, which results from vertical brine fluxes in the lowest layers. The results for $\beta = 1$, 5, and 25 differ only slightly, indicating that most melt water flows vertically through the ice. From the idealized experiment we conclude that changing β has the anticipated effect. A wide spread of values was used for β, and the parametrization has a low sensitivity to changes of β close to our default value of 1. This low sensitivity is an advantage for us because although we lack the data to derive the optimal value of β, having a poor estimate of β will only impact our results slightly.

3.4 Vertical resolution

The impact of changing the vertical resolution is manifold. Δz_0 affects melt water formation, the accuracy of the spatial discretizations, and salinity advection. However,

TCD
8, 1723–1793, 2014

the most direct effect of the resolution on the complex flushing parametrization is that changing Δz_0 changes the distance between parallel connected hydraulic resistances in the ladder circuit, enabling a more refined flow separation.

In the idealized experiment higher resolution leads to a quicker onset of flushing, faster oscillations of the $3\,g\,kg^{-1}$ contour, and a shallower desalination at the surface (see Figs. 6b, 7d, and 8e and f). No strict convergence-like behavior is visible, but at vertical spacings below 2 cm the simulations change only slightly. Given the lack of experimental data or theoretical expectation we can not validate our decision to use a Δz_0 of 1 cm as our default value, but we expect small changes in resolution to not substantially affect results.

3.5 Summary

In the idealized experiment the ratio of deeper penetrating vertical fluxes vs. shallower horizontal fluxes oscillates, which is clearly visible in the $3\,g\,kg^{-1}$ salinity contour. In the absence of gravity drainage salt accumulates in the lowest layers leading to high salinities of up to $20\,g\,kg^{-1}$.

The complex flushing parametrization responds weakly to changes of the parameters β and $\phi_{s,\,melt}$. Changing β has the expected effect, but no theoretical expectations or data are available to determine the optimal value. Accordingly, the chosen default value of 1.0 is highly uncertain and may be off by more than an order of magnitude. However, given the low sensitivity to β even a change of magnitude would not qualitatively change our results. The vertical model resolution has a strong influence on the parametrized flushing with higher resolution leading to quicker oscillations and a shallower desalination at the surface. It is possible that the complex parametrization performs most realistically at a specific layer thickness or that the optimal value of β is resolution dependent, but this can not be determined until more precise data is available.

TCD
8, 1723–1793, 2014

4 Arctic sea ice

In this section we study how SAMSIM simulates the salinity evolution in the Arctic using the complex salinity approach, and compare the model output with ice-core data.

We have decided to limit the study to the Arctic because flooding and the corresponding snow ice formation play a large role in the Antarctic. As explained in Sect. 2.4.4, we treat the flooding parametrizations currently implemented in SAMSIM as ad hoc solutions only suitable for dealing with isolated and sporadic flooding events. Accordingly, we will refrain from studying Antarctic ice until flooding is better understood.

Although a basic understanding of the salinity evolution has existed for many decades, the main processes driving this desalination still pose many unanswered questions. Using a model has the major advantage of being able to track the evolution consistently over long periods of time, while sea-ice cores can only provide snapshots. Simulating the salinity evolution with SAMSIM is an exercise of reproducing a vaguely known result of poorly understood origin. We aim to understand the impact and interactions of the various processes better, while at the same time discovering the limitations of the developed parametrizations or the existence of neglected relevant processes.

4.1 Model setup

To imitate Arctic conditions we use three-hourly ERA-interim radiative fluxes and precipitation to provide the surface conditions for SAMSIM. Nine simulations, each forced with ERA-interim reanalysis data taken from one of nine locations spread over the Arctic, are run from July 2005 till December 2009. The coordinates of the chosen locations from South to North are: 70° N and 0° W, 72° N and 155° E, 75° N and 180° E, 75° N and 0° E, 75° N and 145° W, 80° N and 0° E, 80° N and 90° E, 85° N and 180° E, and 90° N. A simulation period of 4.5 years was chosen because it covers four yearly cycles of growth and melt, which covers the age of most Arctic sea ice (Lietaer et al., 2011).

SAMSIM also requires oceanic boundary conditions in the form of ocean salinity and oceanic heat flux. Due to the scarcity of oceanic heat flux measurements and

TCD
8, 1723–1793, 2014

for simplicity's sake all runs share the same prescribed yearly heat-flux cycle, based loosely on the heat fluxes Huwald et al. (2005a) derived from the SHEBA measurements. The oceanic heat flux is highest in autumn ($14\,W\,m^{-2}$) and lowest in spring ($0\,W\,m^{-2}$). Similarly, a standard ocean salinity of $34\,g\,kg^{-1}$ is used for all runs. The model settings and parameters used are listed in Table 1.

It is important to state that the boundary conditions we use are not necessarily a realistic approximation of the true conditions at the specific locations and time from which we chose the reanalysis data. Not only are the oceanic heat fluxes a strong approximation, the precision of the reanalysis data is limited by the lack of observations in the Arctic. Additionally, the influences of dynamic processes such as frazil formation, lead opening, melt ponds, and ice drift can not be accounted for in the 1-D SAMSIM model. Given the lack of melt pond formation and lead openings SAMSIM will tend to underestimate the amount of melt compared to reality.

4.2 Sample output

To give an example of the model output we have included the salinity evolution of one of the nine simulations for all three salinity approaches (Fig. 9). We chose the simulation forced with reanalysis data from 75° N and 145° W as it has the same forcing during the first growth season as the growth season analyzed in Griewank and Notz (2013). Note that due to the modification to the Rayleigh number (see Sect. 2.2) the salinity evolution of the first growth season shown in Fig. 9 is not identical to the simulated salinity shown in Fig. 9 of Griewank and Notz (2013).

In the sample output the first-year ice survives the first melt season and is followed by three years of multi-year ice. The yearly cycle in sea-ice thickness is clearly visible, with strong inter-annual variations in minimum and maximum ice thickness due to inter-annual variations in the forcing data, such as snow fall. The complex and simple approaches (Fig. 9a and b) both create a detailed salinity profile which evolves during growth and melt with large differences from year to year. In contrast, the prescribed approach (Fig. 9c) has neither inter-annual variability nor a seasonal evolution. As noted

TCD
8, 1723–1793, 2014

in Griewank and Notz (2013), the simple parametrization desalinates slightly stronger during growth, but during the melt season the complex approach loses more salt. In contrast, the prescribed salinity profile results in an increase of bulk salinity over the ice column during melt.

4.3 Ice-core data

We begin analyzing the SAMSIM salinity evolution by comparing the output against salinity characteristics derived from ice-core measurements. Despite its drawbacks, taking ice cores is by far the most wide spread method of measuring sea ice salinity. Gough et al. (2012) provide a thorough overview of statistical and physical sampling issues associated with ice-core salinity measurements. Due to the high horizontal heterogeneity of sea ice we will only use means over multiple ice-cores. It is to be expected that the core measurements underestimate the salinity near the ocean interface due to brine loss (Notz and Worster, 2008).

After over a century of sporadic measurement campaigns beginning with Nansen's Fram expedition, the observational record of Arctic sea-ice salinity is sparse in time and space and no comprehensive compilation of the conducted measurements has been published in the last decades (e.g. Weeks and Lee, 1958; Cox and Weeks, 1974; Nakawo and Sinha, 1981; Eicken et al., 1995). We do not attempt to provide a rigorous model vs. field data comparison in this paper. Instead, we select three characteristic traits of sea-ice salinity to compare SAMSIM's results against. The three traits we compare against are the link between bulk salinity and ice thickness, the first-year salinity evolution from January to June, and the mean multi-year salinity profile from May to September.

4.3.1 Bulk salinity against thickness

The first trait we selected is the link between salinity and thickness which was studied by Cox and Weeks (1974) and Kovacs (1997). For the single growth season studied in

TCD
8, 1723–1793, 2014

Griewank and Notz (2013) the model results agreed well with the fit of Kovacs (1997) for first-year ice up to two meters.

We separate first-year from multi-year ice before comparing the bulk salinity against thickness (Fig. 10). One simulation was singled out and highlighted allowing the reader to track the progress over 4 years as the first-year ice turns into multi-year ice and becomes less saline over time. The simulation which was singled out is the same simulation as shown in Fig. 9.

Both first-year and multi-year ice show a distinctly different behavior during growth and melt. The gradual transition from growth to melt is visible as a drop in bulk salinity at a constant thickness. A closer examination reveals that a slight thickness increase is visible in many simulations before ablation sets in. This bump in ice thickness arises from SAMSIM's definition of sea-ice which includes melting snow that has turned into slush (for details see Sect. 2.3.1). That this little bump appears at the end of the downward drop signals that until then no flushing has occurred. From that we can conclude that gravity drainage is what causes the drop in salinity.

Ice thinner than 20 cm has a wide spread in bulk salinity caused by melting and flooding at the onset of the growth season. The simulated first-year ice thicker than 20 cm agrees well with the empirical results of Cox and Weeks (1974) and Kovacs (1997) during growth, with the model having a higher salinity. This bias is especially high for ice thinner than 0.5 m, which may be partially due to the fact that the underestimation of bulk salinity due to brine loss is higher for thin cores. After the onset of melt the bulk salinities are comparable to the estimates of Cox and Weeks (1974), which were based on a limited amount of cores which were at least a meter thick.

As expected multi-year sea ice shows a much smaller range of bulk salinities (Fig. 10b). During growth the bulk salinities show no coherent dependence on thickness, but during melt there appears to be a slight linear dependence on thickness going from $1\,g\,kg^{-1}$ at 0.5 m to $2\,g\,kg^{-1}$ at 2.5 m. This is not far off from the estimation of Cox and Weeks (1974).

TCD
8, 1723–1793, 2014

In conclusion, the modelled thickness–salinity relationship of growing first-year ice agrees well with the empirical fits to measurements of both Cox and Weeks (1974) and Kovacs (1997). Although growing multi-year ice tends to be less salty when thicker, there is no uniform dependence on thickness. Both melting first-year and multi-year ice show a linear dependence of salinity on thickness. The transition from growing to melting ice leads to a loss in bulk salinity at a constant thickness which is caused by gravity drainage in the warming ice.

4.3.2 First-year salinity evolution

The second trait of the modeled salinity we evaluate with core data is the evolution of first-year ice salinity from January until June. A longer time frame was not possible due to data availability, but none the less the period allows us to study the salinity changes after gravity drainage is mostly restricted to the lower layers. We use the ice-core data taken as part of the Seasonal Ice Zone Observing Network and the Alaska Ocean Observing System by the sea-ice research group at the Geophysical Institute at the University of Fairbanks from 1999–2011 (Eicken et al., 2012). The great advantage of these measurements other than the shear number of cores taken is that by measuring repeatedly over a decade a large spread of conditions were captured. After rejecting all cores which did not include an ice thickness measurement or contained gaps in the salinity profile, a total of 86 first-year profiles remained between January and June.

The comparison of the model salinity against the Barrow cores is not ideal because SAMSIM is forced with conditions from throughout the Arctic while the cores where all taken close to the Alaskan coast as part of an ongoing effort to understand and alleviate the impact of changing sea-ice on the human settlements along the coast (Druckenmiller et al., 2009). However, as we will show in the following subsection on interannual salinity variability the salinity variations resulting from atmospheric conditions are strongest in the upper most 20 cm (Sect. 4.5). Because of this, we believe that the comparison should work well for the lower 80 % of the ice.

TCD
8, 1723–1793, 2014

To compare the core profiles against the model profiles both are first normalized to a depth of 0 to 1 before averaging over time. Often the salinity measurements did not extend all the way to the bottom of the ice, in which case the lowest measurement was extrapolated downwards. This extrapolation will contribute to the underestimation of salinity at the ice-ocean interface common to ice cores. We group the 86 core measurements into three bins of similar size based on the dates they were taken. The first bin spans from January to March (27 cores), the second from April to May (29 cores), and the final bin contains the remaining 29 cores taken in June.

As expected, even though the core profiles have a sharp increase of salinity at the ice-ocean interface they are still less saline at the ice-ocean boundary than SAMSIM (Fig. 11). Other than the top and bottom 10 % of the ice thickness, the simulated salinity profiles and the Barrow cores never differ by more than $2\,\mathrm{g\,kg^{-1}}$, which is in itself a mentionable model feat.

Other than the general agreement this comparison highlights some limitations of SAMSIM's complex salinity approach. One of these limitations is that flushing and snow melt by design lead to a zero salinity at the surface, which is clearly not present in the core data (Fig. 11). However, it is likely that core values at the surface would be lower if the sampling resolution were higher than the 2.5 to 5 cm used.

This total desalination at the surface is rooted in two of SAMSIM's design choices. The first design choice is that the snow layer in SAMSIM has zero salinity, and that melting snow forms slush which is treated as sea ice. Accordingly, when snow melts the top ice layer will consist of melted snow slush and be absolutely salt free. The second design choice which leads to zero salinity at the surface is the implementation of flushing in SAMSIM. One of the core assumptions of the complex flushing parametrization is that the melt water leaving the top ice layer has a brine salinity determined by the liquidus relationship. Accordingly, as the brine salinity of the top ice layer is by definition always higher than the bulk salinity of the top ice layer, flushing always results in zero salinity at the surface over time as shown by the idealized flushing experiments (Sect. 3).

TCD
8, 1723–1793, 2014

The second distinct difference between model and core salinity is that SAMSIM has a high surface salinity with a very strong salinity gradient (Fig. 11b). The sharp salinity gradient which occurs in the top few model layers could be a numerical artifact arising from SAMSIM's semi-adaptive grid. The first centimeters of ice are formed when only few layers are active, which might be insufficient to parametrize gravity drainage. A different explanation is snow wicking, a process which transfers some of the surface salinity into the snow layer. In the model wicking only occurs when melt water forms in the top ice layer beneath snow.

The third discrepancy between the cores and SAMSIM is that the bulk salinity in the upper 40 % does not change from January–March to April–May in the model. There are many possible explanations for this discrepancy, such as the non-ideal comparison itself, insufficient simulations or core measurements, and errors of the core salinity measurements. Another explanation is that the model is unable to simulate the salinity evolution correctly close to the surface during winter. A likely candidate to explain that the salinity remains constant near the surface is that the gravity drainage parametrization desalinates too quickly during growth. The modeled salinity is quickly reduced to $5\,\mathrm{g\,kg^{-1}}$ after which it stabilizes, instead of a less strong initial desalination followed by a gradual desalination over time (Fig. 11). The discrepancy between model and data could also arise from the neglect of frazil or pancake ice formation in SAMSIM. It is also possible that the freeboard plays an important role, and that brine from above the waterline drains away by an unknown mixture of gravity drainage or flushing. The differences between the cores and SAMSIM as well as our poor understanding of what happens during flooding indicates that unknown yet relevant brine movements may occur at the ice-snow interface. Despite the indirect model to data comparison and the three discrepancies in the salinity evolution discussed, SAMSIM successfully captures the general shape and magnitude of the three core-derived salinity profiles.

TCD
8, 1723–1793, 2014

4.3.3 Multi-year salinity profile

The final and most well documented trait we select to compare is the mean multi-year salinity profile. The most widely used multi-year profile in the sea-ice modelling community is based on 40 ice cores taken at the drifting ice station A in 1958 (Schwarzacher, 1959) from May to September. Although later studies have incorporated additional measurements (e.g. Cox and Weeks, 1974; Eicken et al., 1995), the basic shape has remained similar. The fitted bulk salinity profile of Schwarzacher (1959) on a normalized vertical coordinate z from zero to one

$$S_{\mathrm{bu}}(z) = 1.6(1 - \cos)(\pi z^{\frac{0.407}{0.573+z}})$$

is used in the 1-D models of Maykut and Untersteiner (1971) and Bitz and Lipscomb (1999). As the Schwarzacher cores were all taken from May to September, and the eight multi-year cores from Barrow were also taken in summer, we compare the normalized Barrow cores and Schwarzacher profile against the mean of SAMSIM from May to September.

Although the fitted Schwarzacher profile has a $3.2\,\mathrm{g\,kg^{-1}}$ salinity at the ice-ocean interface (Fig. 12), in the measurements an increase is clearly visible, similar to the salinity increase of the eight multi-year salinity cores taken at Barrow. Due to this ignored increase and the repeatedly mentioned salinity loss in cores we only compare against the upper 90 % the Schwarzacher profile. Although this comparison from SAMSIM to field data is far from perfect, it is the closest we can come to evaluating the flushing parametrization until controlled laboratory measurements are available.

We compare the May to September mean of all normalized multi-year SAMSIM profiles against the profile of Schwarzacher (1959) and the Barrow cores, which all share a similar magnitude and shape in the upper 90 % (Fig. 12). Both SAMSIM and the Barrow cores have a slight maximum at a depth of 40 %, which indicates that the complex flushing parametrization predicts the desalination depth reasonably correctly. Despite the slight overestimation of salinity in the top 40 %, the good agreement between SAMSIM and ice-core data is a very positive and non-trivial result, given that the complex

TCD
8, 1723–1793, 2014

flushing parametrization contains large parameter uncertainties and was developed from scratch without any data available to tune the free parameter β.

Between the depth fractions of 0.5 and 0.8, SAMSIM and the Barrow cores show a slight salinity decrease with depth while the Schwarzacher profile has a slight increase (Fig. 12). The differences between the model and the ice-core data is of similar magnitude to the differences caused by using different values of α and R_{crit} obtained from the optimization process mentioned in Sect. 2.2. The Barrow cores and SAMSIM both have a sharp salinity increase in the lowest 10 %. That the model is saltier at the ice-ocean boundary is expected due to brine loss during coring and a lower spatial resolution of the measurements compared to the model.

4.3.4 Summary

According to SAMSIM there is a clear link between ice thickness and bulk salinity in growing first-year ice as described by Kovacs (1997). However, after the ice stops growing, gravity drainage in the warming ice causes a thickness independent desalination. Both melting first-year and multi-year ice show an approximately linear dependence of bulk salinity on ice thickness as suggested by Cox and Weeks (1974). The mean multi-year salinity profile of SAMSIM from May to September agrees well with the core data of Schwarzacher (1959) and Barrow. The salinity evolution in first-year ice in SAMSIM is comparable to ice-core measurements at Barrow (Eicken et al., 2012). However, in contrast to the Barrow core data the modeled salinity close to the ice surface remains constant from January–March to April–May, indicating that brine fluxes occur close to the surface which are poorly captured by the complex set of parametrizations.

All comparisons between SAMSIM and ice core data show that SAMSIM captures the general salinity evolution well, both qualitatively and quantitatively. Keep in mind that no tuning was used to reach these results and that all parametrizations were developed without any field data. Additionally, all parametrizations were developed separately, with no regard to possible interactions. From the comparison to ice cores we

TCD
8, 1723–1793, 2014

conclude that our parametrizations and understanding of desalination processes are sufficient to use SAMSIM as a tool to study Arctic sea ice.

4.4 Mean salinity evolution

In this subsection we analyze the mean salinity evolution of the complex approach. In total the model simulations yield 36 years of sea-ice growth and melt. Of those 36 years 21 years are multi-year ice and 15 are first-year ice. Of the 15 years of first-year ice 8 years end in open water while 7 form multi-year ice in the following year.

To process and visualize the salinity evolution we first normalize all salinity profiles of the model output between 0 and 1. This allows averaging over multiple normalized profiles and simplifies comparing profiles of varying thicknesses. To resolve the mean annual cycle we sort all first-year and multi-year profiles into monthly bins beginning in September, which we then average (Fig. 13). A side effect of this averaging approach is that when there is no ice in the model output this output does not affect the mean salinity profile. As a consequence the mean August profile consists mostly of first-year ice which will turn into multi-year ice the following year and there is a smooth transition from the August first-year profile to the September multi-year profile. This selection effect is clearly visible when comparing the mean ice thickness of all first-year simulations excluding ice free output against the mean thickness of first-year ice which turns into multi-year ice next September (Fig. 14).

During the growth season the salinity of the first-year ice decreases to $5\,\mathrm{g\,kg^{-1}}$ after about two months with a sharp increase to $10\,\mathrm{g\,kg^{-1}}$ in the upper 5 % of the ice thickness (Fig. 13a). As the ice grows thicker the lower layers retain less salt, indicating that on average the lower growth speed of thicker ice does lead to a reduced amount of salt being retained as was proposed by Cox and Weeks (1975) and Wettlaufer et al. (1997). In contrast, in our previous study using the same gravity drainage parametrization, albeit with a different definition of the Rayleigh number, this behaviour of retaining less salt at slower growth speeds was only present in idealized experiments but not in the single growth season studied (Griewank and Notz, 2013).

TCD
8, 1723–1793, 2014

The salinity profile remains pretty stable between November and April, followed by a slight desalination in May at the onset of melt. The desalination accelerates during June and July until the upper 80 % of the ice have a salinity below $3\,g\,kg^{-1}$ (Fig. 13b). The influence of flushing is clearly visible by the total loss of salt at the surface from June onwards. Given that the maximal salinity occurs between an ice-depth fraction of 0.2 and 0.4, the desalination caused by flushing in the model occurs mostly in the top third of the ice. Although there is only little and indirect experimental evidence of gravity drainage occurring as the ice warms (e.g Widell et al., 2006; Jardon et al., 2013) the salinity reduction in the lower half of the ice from April to June shows that gravity drainage is active in SAMSIM during the onset of melt. This desalination is consistent with results from idealized experiments we conducted that show a reduction of bulk salinity from above $5\,g\,kg^{-1}$ to below $3\,g\,kg^{-1}$ from gravity drainage when sea-ice begins to warm (Griewank and Notz, 2013).

At the end of the melt season the multi-year ice salinity is lowest (Fig. 13c). While the surface salinity remains low the newly formed ice at the bottom retains over $5\,g\,kg^{-1}$. During the melt season the lower half of the ice is desalinated by gravity drainage while flushing maintains the low surface salinity. That this desalination is not only due to the loss of the saltier lower layers through melt is visible in the curve that develops in the lower half of the normalized profile. This curve is also visible in the Barrow core data shown in Fig. 12. With the exception of the gravity drainage during melt the overall multi-year salinity agrees well with expectations already voiced by Cox and Weeks (1974).

For readers interested in analytical approximations of the mean first-year and multi-year profiles we offer two functions $S_{\mathrm{bu,\,fy}}(z)$ and $S_{\mathrm{bu,\,my}}(z)$. Both are a function of the normalized ice depth $0 \leq z \leq 1$ and are shown in Fig. 15 along with the mean SAMSIM profiles. The fitted first-year ice profile is

$$S_{\mathrm{bu,\,fy}}(z) = \frac{az}{1.0 + bz^2} + c \tag{1}$$

TCD
8, 1723–1793, 2014

for $a = 1.543$, $b = -0.9477$, $c = 4.517$ and the fitted multi-year ice profile is

$$S_{\mathrm{bu,my}}(z) = a(1 - e^{bz}) + c(1 - e^{dx}) \quad (2)$$

with $a = -2.874 \cdot 10^{-18}$, $b = 43.52$, $c = 8.599$, $d = -1.141$.

The transition from first-year to multi-year ice over the melt season can be approximated by a time dependent combination of the two profiles, in the form

$$S_{\mathrm{bu}}(z,t) = (1-t) \cdot S_{\mathrm{bu,my}}(z) + t \cdot S_{\mathrm{bu,my}}(z)$$

for $t = 0$ at the beginning of the melt season in June and $t = 1$ at the onset of growth in September.

4.5 Variability

While the previous subsection studied the mean salinity properties, in this subsection we will take a brief look at the salinity variability in SAMSIM using the complex approach. The model variability arises from two sources, the main one being the atmospheric forcing. Although the location at which the reanalysis data was selected has the largest impact, interannual variability ensures that all 36 years of simulated sea ice have a unique forcing. The second source for variability is the initial ice conditions at the beginning of the growth season. This second source only applies to the 21 years of multi-year ice, since all first-year ice grows from ice-free water. The variance of the model can not be directly compared to ice-core variability, because the variability in ice cores additionally contains a large amount of variability due to small scale horizontal heterogeneity (Gough et al., 2012).

To visualize the variability we have plotted all normalized salinity profiles at two dates in time, as well as the mean over all profiles at that time point in Fig. 16. With few exceptions the first-year ice only deviates a few g kg^{-1} from the mean in the lowest 80 % of the ice. However, at the surface the spread is much higher, with values reaching from 0 to above 10 g kg^{-1} (see Fig. 16a and b). There are two main reasons for the

TCD
8, 1723–1793, 2014

higher variability at the surface. The first is that after 10 to 20 cm of ice has formed, the variability of the atmospheric forcing is severely dampened before it reaches the ice-ocean interface. As a result, the ice formed after the initial 10–20 cm grows under roughly similar conditions in all simulations. The second reason is that flooding and flushing both occur mainly at the surface of the ice. That such a similar high variability near the surface is not visible in the multi-year ice is because both processes are far less likely to occur in multi-year ice during the winter than in first-year ice. Farther south where first-year ice seldom survives the melt season, rainfall and above-freezing surface temperatures occur during the growth season, both of which can cause flushing. As the first-year ice is less thick, strong snow fall which slows ice growth can lead to flooding more easily than in multi-year ice.

As all multi-year ice has experienced at least one melt season, it is not surprising that multi-year simulations have a salinity of zero at the surface (Fig. 16c and d). That all 21 years have zero surface salinity shows that flooding of multi-year ice does not occur in any of the simulations. Most of the variability in multi-year ice arises from the different ice thickness and salinity of the ice at the end of the melt season. The spikes visible in roughly 4 simulations between 0.4 and 0.6 in the November profiles arise from sudden quick growth in the beginning of the growth season beneath comparably fresh ice (Fig. 16c). This growth can be quicker than in first-year ice of similar thickness due to the following reasons. The first reason is that by the time first-year ice reaches the same thickness, it has likely accumulated an insulating snow layer which slows ice growth. Secondly, the fresher multi-year ice has a higher thermal conductivity and lower thermal capacity which enhances heat transport from the ice-ocean interface to the ice-atmosphere boundary.

Over the next half year the profiles are smoothed out and the salinity sinks to 7 g kg^{-1} or lower except in the lowest 10 % (Fig. 16d). Visible in both first-year ice and multi-year ice is that the salinity in the lowest layers is higher in November during ice growth than in April.

TCD
8, 1723–1793, 2014

In conclusion, the variability in first-year ice is strongest at the surface and arises from the atmospheric forcing, while the variability in multi-year ice is mostly due to the thickness of the ice at the beginning of the growth season. A third possible source of variance is the variation in the oceanic heat flux. This is not included in this study as all simulations share the same prescribed annual cycle of oceanic heat flux.

5 Impact of parametrizing salinity

While the previous section focused on the salinity evolution and the processes which drive it, this section aims to quantify how parametrizing salinity affects sea-ice properties relevant to the climate system. We address this question, which is highly relevant to modellers seeking to improve climate models, by using the same runs used in the previous section (see Sect. 4.1).

To asses the total impact of parametrizing salinity in a climate model it is not sufficient to quantify the impact on the sea ice itself. It is also necessary to determine resulting feedbacks with the ocean and atmosphere. So far the only coupled model featuring a partially parametrized salinity is the NEMO-LIM model which uses a prescribed atmospheric forcing. Using the NEMO-LIM model Vancoppenolle et al. (2009) found that the large-scale sea-ice mass balance and the upper ocean characteristics are quite sensitive to sea-ice salinity. Salinity variations introduced to NEMO-LIM increased sea ice volume by up to 28 % in the Southern Hemisphere because changes to the ice-ocean interactions stabilized the ocean leading to a reduced oceanic heat flux. In the Arctic the ocean stratification was not influenced by the implemented sea-ice variations, but Vancoppenolle et al. (2009) discovered increases in ice thickness of up to a meter due to changes of the sea-ice thermal properties.

From Vancoppenolle et al. (2009) we conclude that in the Arctic the oceanic feedbacks will be small owing to the stable stratification of the Arctic Ocean. Although the atmospheric feedbacks remain unknown, we can use SAMSIM's more advanced salinity

TCD
8, 1723–1793, 2014

parametrizations with a much higher spatial and temporal resolution to take a more detailed look at how the salinity evolution affects the sea ice.

A further piece of information needed to weigh introducing salinity parametrizations into a coupled model is the resulting increase in computational cost and code complexity. As there are a number of options where to invest additional computational resources (e.g. increasing spatial resolution, more ice thickness categories per grid cell, more complex radiation schemes) it would be ideal to give an estimation of the computational increase along with the estimated improvement so modelers can gauge where to invest free resources most efficiently. A brief description of the numerical costs associated with the salinity approaches and the general issue of code complexity can be found in Sect. 2.5.

To quantify the impact of parametrizing salinity we compare quantities of the nine reanalysis forced simulations using the three salinity approaches introduced in Sect. 2.5. The specific quantities we use based on their importance for the climate system are the same four used in Griewank and Notz (2013). These are the ice thickness, the freshwater column stored in the ice and snow, the thermal resistance R_{th}, and the total enthalpy H integrated over the whole ice and snow column. Each of the nine runs is evaluated separately over the full 4.5 simulation years to ensure that opposing biases at different locations do not average out.

The metrics we use to compare the time dependent quantities against each other are a time integrated ratio and a time integrated, weighted absolute difference. The ratio r of the quantity $x_i(t)$ using the salinity approach i against the same quantity using the different salinity approach $x_j(t)$ over the simulated 4.5 years is calculated as

$$r = \frac{\int_{t=0}^{t=4.5\,\mathrm{a}} x_i(t)\mathrm{d}t}{\int_{t=0}^{t=4.5\,\mathrm{a}} x_j(t)\mathrm{d}t}.$$

TCD
8, 1723–1793, 2014

The second metric used, the weighted absolute difference d, is determined by

$$d = \frac{\int_{t=0}^{t=4.5\,\mathrm{a}} x_i(t) - x_j(t)\mathrm{d}t}{\int_{t=0}^{t=4.5\,\mathrm{a}} x_j(t)\mathrm{d}t}$$

and is a measure of how large the differences are between the two quantities at each time step compared to the total value of the second quantity. The ratio is chosen to indicate if and by how much x_i is greater or smaller than x_j over time, while the absolute difference is chosen to detect compensating errors not apparent in the ratio. We quantify the impact by comparing the simple and prescribed approach against the complex approach.

The computed ratios for each simulation reveal that the prescribed approach with few exceptions leads to a lower ice thickness, freshwater column, thermal resistance, and total enthalpy than the complex approach (Fig. 17). Ratios range from 0.90 to 1.07. The mean over all ratios and quantities of the prescribed approach is 0.977, accordingly the quantities of the complex approach are 2.3 % higher on average. The ratios of the simple approach have a slightly lower spread and are on average higher with a mean of 1.026.

The absolute differences paint a similar picture, with the prescribed approach having a slightly larger spread with differences up to 11 % (Fig. 18). On average the simple approach has slightly lower differences with a mean of 4.3 % in comparison to the prescribed mean of 4.5 %. Because the absolute differences are only slightly larger than the ratios, we can deduce that most of the discrepancy between two simulations is in one direction.

Given that the prescribed approach does not distinguish growing from melting ice and that the prescribed profile was not optimized or tuned in any way, the simulated ice properties using the prescribed approach are unexpectedly close to the complex approach. We also expected the prescribed approach to have a wider spread when compared to the complex approach, because the prescribed approach treats all ice the

TCD
8, 1723–1793, 2014

same regardless of its history while the complex approach is dependent on previous conditions (as visible in Fig. 9).

From our results we conclude that the possible improvements achievable by fully parametrizing salinity in the Arctic are not worth the numerical costs, especially because the impact of parametrizing salinity will be smaller when fewer layers are used. Instead we recommend using either a prescribed profile or a hybrid approach. The salinity approach used by Vancoppenolle et al. (2009) is such a hybrid, in which the total bulk salinity of the whole column is parametrized and the salinity profile is prescribed based on the bulk salinity. Prescribed profiles can also be thickness, time, location, or age dependent. Equations (1) and (2) for first-year and multi-year ice are examples of an age dependent profiles, while the prescribed salinity profile used in SAMSIM is a thickness depenent profile. If a model can distinguish first-year and multi-year ice this information could also be used to prescribe the salinity, as is done in the time dependent method proposed at the end of Sect. 4.4.

6 Summary and conclusions

We have incorporated surface melt, flooding, and flushing into SAMSIM. In contrast to the thermodynamic models derived from Maykut and Untersteiner (1971), such as Bitz and Lipscomb (1999) and Huwald et al. (2005b), surface melt in SAMSIM is implemented as a two stage process. The first stage is the conversion of snow to slush followed by the second stage of surface ablation by melt water runoff. All desalination processes are parametrized in two different ways in SAMSIM. The complex parametrizations calculate brine fluxes and are physically consistent, while the simple parametrizations attempt to imitate the effects of the complex parametrizations with less numerical overhead.

SAMSIM is the only 1-D thermodynamic sea-ice model other than the 1-D LIM model of Vancoppenolle et al. (2007) which has a fully prognostic salinity. In contrast to the flushing parametrization of Vancoppenolle et al. (2007), the complex flushing

TCD
8, 1723–1793, 2014

parametrization of SAMSIM explicitly includes both horizontal and vertical brine movements. A detailed discussion of why the complex gravity drainage parametrization of SAMSIM agrees better than the gravity drainage of LIM 1-D with both theoretical and numerical expectations is included in Griewank and Notz (2013). The complex flooding parametrization based on the results of Maksym and Jeffries (2000) is an ad hoc solution as the current understanding of flooding is insufficient to develop a more realistic parametrization. Nevertheless, SAMSIM is the first 1-D model to include flooding as well as flushing and gravity drainage, and the flooding parametrization does capture the basics of flooding and produces snow ice with reasonable salinities in a physically consistent manner.

Under idealized conditions, the complex flushing parametrization leads to oscillations of the salinity profile close to the surface. If gravity drainage is deactivated flushing also leads to a strong increase of salinity close to the ice-ocean interface. Although we do not have data available to determine optimal values of the ratio of vertical to horizontal hydraulic resistance β and the melt solid fraction $\phi_{\mathrm{s,\,melt}}$, sensitivity experiments show that the flushing parametrization is only weakly sensitive to changes close to the default values. At higher vertical resolution the flushing onset occurs sooner and the salinity oscillations have a higher frequency.

We study the salinity evolution of Arctic sea ice using 36 years of SAMSIM output. To imitate Arctic conditions we force SAMSIM with ERA-interim reanalysis precipitation and radiation fluxes from throughout the Arctic. The 36 years are separated into 15 years of first-year and 21 years of multi-year sea-ice and then compared against ice-core data. The mean multi-year salinity profile of Schwarzacher (1959) and the salinity evolution of first-year ice cores from Barrow Alaska agree well with SAMSIM simulations. However, while the first-year ice-core salinity at the surface decreases from January to May, the modelled salinity at the surface remains constant until the onset of melt. This discrepancy indicates that brine fluxes close to the ice-snow boundary are captured poorly by SAMSIM. Possible reasons for this discrepancy are discussed in detail in Sect. 4.3.2.

TCD
8, 1723–1793, 2014

We deduce from the 36 years of simulated sea-ice that ice thickness is a good indicator of bulk salinity for growing first-year ice. The model results agree well with the empirical results of Cox and Weeks (1974) and Kovacs (1997). That the modeled bulk salinities of thin ice are higher than the ice-core data is at least partially due to the fact that brine loss during coring is especially high from thin and more saline ice. The transition from growth to melt is accompanied by a 1.5–4 g kg^{-1} reduction of bulk salinity caused by gravity drainage before the onset of flushing. This onset of gravity drainage as the ice warms is consistent with earlier findings by Griewank and Notz (2013) and Jardon et al. (2013). The onset contradicts the general melt evolution depicted by Eicken et al. (2002) in which gravity drainage sets in at the end of the melt season. In general thicker multi-year ice tends to be fresher, but during growth the bulk salinity increases with thickness. During melt both multi-year and first-year ice have a linear relationship of bulk salinity and thickness as Cox and Weeks (1974) hypothesized on a limited set of cores, but the slope of the linear relationship in the model is steeper than that proposed by Cox and Weeks (1974).

Our results show that the largest interannual variations of salinity occur at the surface of first-year ice and are caused by rain, surface melt, and flooding. In contrast, the lower 80 % of the salinity profile of first-year ice are similar to each other, despite being forced with reanalysis data taken from different locations and years. The multi-year ice profiles vary depending on the ice thickness at the onset of growth and become more similar over the growth season.

We compare the ice thickness, freshwater column, thermal resistance, and total stored energy of the nine 4.5 year long simulations of Arctic sea-ice using the three different salinity approaches against each other. Although certain quantities differ by up to 11 % for a specific simulation, on average the differences between the complex salinity approach and the other approaches are below 5 %. The simple approach has a slightly smaller difference compared to the complex approach than the prescribed approach (Fig. 18), but the prescribed approach has a better ratio (Fig. 17). Given that the strong arctic halocline should prohibit strong ice-ocean feedbacks, we conclude

TCD
8, 1723–1793, 2014

that fully parametrizing the temporal sea-ice salinity evolution in the Arctic for climate models is not worth the computational cost and increase in code complexity. Instead, we recommend using a parametrized-prescribed hybrid such as that proposed by Vancoppenolle et al. (2009), which parametrizes the evolution of the bulk salinity of the whole ice column and prescribes an empirical salinity profile based on the bulk salinity. While the parametrization of Vancoppenolle et al. (2009) also captures some seasonal variations, the most crucial aspect of a parametrized-prescribed hybrid is the ability to distinguishing multi-year from first-year ice. This aspect can also be achieved by tracking the ice age. Once the model is able to distinguish first-year from multi-year ice, empirical profiles of first-year and multi-year, such as the mean normalized profiles shown in Fig. 15 can be prescribed. The multi-year profile of Schwarzacher (1959) underestimates the mean salinity profile, as it is based on cores taken from May to September during which the salinity is lower (Fig. 13). A smooth transition from first-year to multi-year ice can be achieved by linearly transitioning from the first-year to the multi-year profile as discussed in Sect. 4.4. Further refinement can be achieved by taking the annual cycle into account (Fig. 13), the ice thickness (Fig. 10), and the sea ice location.

Comparisons to laboratory and field salinity measurements have shown that the parametrized brine fluxes in SAMSIM are a reasonable approximation of reality. SAMSIM's semi-adaptive grid is convenient when studying processes which occur close to the ice-atmosphere or ice-ocean boundary, as it avoids numerical diffusion through layer advection in the surface and bottom layers. All dissolved tracers in brine can be easily advected similar to salt, and the gas volume fraction in each layer can be used to compute outgassing and uptake. Thanks to these properties SAMSIM is a valuable tool to study small-scale thermodynamic and other aspects of sea ice which are affected by brine dynamics.

Acknowledgements. We would like to thank T. Mauritsen and J. Marotzke for commenting on the manuscript, the ECMWF for providing the ERA-interim reanalysis data freely for research, and the Barrow Sea Ice Observatory for hosting their ice-core data openly online.

TCD
8, 1723–1793, 2014

The service charges for this open access publication
have been covered by the Max Planck Society.

References

Bitz, C. M. and Lipscomb, W. H.: An energy-conserving thermodynamic model of sea ice, J. Geophys. Res., 104, 15669–15677, doi:10.1029/1999JC900100, 1999. 1726, 1732, 1735, 1757, 1766

Coleou, C. and Lesaffre, B.: Irreducible water saturation in snow: experimental results in a cold laboratory, Ann. Glaciol., 26, 64–68, 1998. 1733

Cox, G. and Weeks, W.: Brine Drainage and Initial Salt Entrapment in Sodium Chloride Ice, Tech. rep., DTIC Document, Hanover, N.H., U.S. Army Cold Regions Research and Engineering Laboratory, 1975. 1759

Cox, G. F. and Weeks, W. F.: Salinity variations in sea ice, J. Glaciol., 13, 109–120, 1974. 1752, 1753, 1754, 1757, 1758, 1760, 1768, 1785

Druckenmiller, M. L., Eicken, H., Johnson, M. A., Pringle, D. J., and Williams, C. C.: Toward an integrated coastal sea-ice observatory: system components and a case study at Barrow, Alaska, Cold Reg. Sci. Technol., 56, 61–72, 2009. 1754

Eicken, H., Lensu, M., Lepparanta, M., Tucker, W. B., Gow, A. J., and Salmela, O.: Thickness, structure, and properties of level multiyear ice in the Eurasian sector of the Arctic-ocean, J. Geophys. Res., 100, 22697–22710, doi:10.1029/95JC02188, 1995. 1733, 1736, 1737, 1752, 1757

Eicken, H., Krouse, H., Kadko, D., and Perovich, D.: Tracer studies of pathways and rates of meltwater transport through Arctic summer sea ice, J. Geophys. Res., 107, 8046, doi:10.1029/2000JC000583, 2002. 1725, 1732, 1734, 1737, 1748, 1768

Eicken, H., Gradinger, R., Kaufman, M., and Petrich, C.: Sea-ice core measurements (SIZONET), UCAR/NCAR – CISL – ACADIS, doi:10.5065/D63X84KG, 2012. 1754, 1758, 1787

Flocco, D. and Feltham, D. L.: A continuum model of melt pond evolution on Arctic sea ice, J. Geophy. Res., 112, C08016, doi:10.1029/2006JC003836, 2007. 1725

TCD
8, 1723–1793, 2014

Gough, A. J., Mahoney, A. R., Langhorne, P. J., Williams, M. J. M., and Haskell, T. G.: Sea ice salinity and structure: a winter time series of salinity and its distribution, J. Geophys. Res., 117, C03008, doi:10.1029/2011JC007527, 2012. 1752, 1761

Griewank, P.: A 1-D model study of brine dynamics in sea ice, Ph.D. thesis, University of Hamburg, Germany, 2014. 1730

Griewank, P. J. and Notz, D.: Insights into brine dynamics and sea ice desalination from a 1-D model study of gravity drainage, J. Geophys. Res., 118, 3370–3386, doi:10.1002/jgrc.20247, 2013. 1724, 1725, 1727, 1728, 1729, 1730, 1736, 1742, 1743, 1751, 1752, 1753, 1759, 1760, 1764, 1767, 1768

Hunke, E. C., Notz, D., Turner, A. K., and Vancoppenolle, M.: The multiphase physics of sea ice: a review for model developers, The Cryosphere, 5, 989–1009, doi:10.5194/tc-5-989-2011, 2011. 1725

Huwald, H., Tremblay, L. B., and Blatter, H.: Reconciling different observational data sets from Surface Heat Budget of the Arctic Ocean (SHEBA) for model validation purposes, J. Geophys. Res., 110, 2156–2202, doi:10.1029/2003JC002221, 2005a. 1751

Huwald, H., Tremblay, L.-B., and Blatter, H.: A multilayer sigma-coordinate thermodynamic sea ice model: validation against Surface Heat Budget of the Arctic Ocean (SHEBA)/Sea Ice Model Intercomparison Project Part 2 (SIMIP2) data, J. Geophys. Res., 110, C05010, doi:10.1029/2004JC002328, 2005b. 1766

Jardon, F., Vivier, F., Vancoppenolle, M., Lourenco, A., Bouruet-Aubertot, P., and Cuypers, Y.: Full-depth desalination of warm sea ice, J. Geophys. Res., 118, 1–13, 2013. 1725, 1760, 1768

Jeffery, N., Hunke, E. C., and Elliott, S. M.: Modeling the transport of passive tracers in sea ice, J. Geophys. Res., 116, C07020, doi:10.1029/2010JC006527, 2011. 1725

Jeffries, M. O., Roy Krouse, H., Hurst-Cushing, B., and Maksym, T.: Snow-ice accretion and snow-cover depletion on Antarctic first-year sea-ice floes, Ann. Glaciol., 33, 51–60, 2001. 1740

Kovacs, A.: Sea Ice. Part 1. Bulk Salinity Versus Ice Floe Thickness, CRREL Report, 96-7, Hanover, N.H., U.S. Army Cold Regions Research and Engineering Laboratory, 1997. 1752, 1753, 1754, 1758, 1768, 1785

Lietaer, O., Deleersnijder, E., Fichefet, T., Vancoppenolle, M., Comblen, R., Bouillon, S., and Legat, V.: The vertical age profile in sea ice: theory and numerical results, Ocean Model., 40, 211–226, 2011. 1750

TCD
8, 1723–1793, 2014

Light, B., Grenfell, T. C., and Perovich, D. K.: Transmission and absorption of solar radiation by Arctic sea ice during the melt season, J. Geophys. Res., 113, C03023, doi:10.1029/2006JC003977, 2008. 1729
Maksym, T.: Brine percolation, flooding and snow ice formation on Antarctic sea ice, Ph.D. thesis, University of Alaska Fairbanks, USA, 2001. 1740
Maksym, T. and Jeffries, M. O.: A one-dimensional percolation model of flooding and snow ice formation on Antarctic sea ice, J. Geophys. Res., 105, 26313–26331, 2000. 1740, 1742, 1767
Maksym, T. and Jeffries, M. O.: Phase and compositional evolution of the flooded layer during snow-ice formation on Antarctic sea ice, Ann. Glaciol., 33, 37–44, 2001. 1740, 1741
Maykut, G. A. and Untersteiner, N.: Some results from a time-dependent thermodynamic model of sea ice, J. Geophys. Res., 76, 1550, doi:10.1029/JC076i006p01550, 1971. 1725, 1757, 1766
Nakawo, M. and Sinha, N. K.: Growth-rate and salinity profile of 1st-year sea ice in the high Arctic, J. Glaciol., 27, 315–330, 1981. 1752
Notz, D.: Thermodynamic and fluid-dynamical processes in sea ice, Ph.D. thesis, Univ. of Cambridge, Cambridge, UK, 2005. 1730
Notz, D. and Worster, M. G.: In situ measurements of the evolution of young sea ice, J. Geophys. Res., 113, C03001, doi:10.1029/2007JC004333, 2008. 1752
Notz, D. and Worster, M. G.: Desalination processes of sea ice revisited, J. Geophys. Res., 114, C05006, doi:10.1029/2008JC004885, 2009. 1736
Notz, D., McPhee, M., Worster, M., Maykut, G., Schlünzen, K., and Eicken, H.: Impact of underwater-ice evolution on Arctic summer sea ice, J. Geophys. Res., 108, 3223, doi:10.1029/2001JC001173, 2003. 1737
Pedersen, C. A., Roeckner, E., Luthje, M., and Winther, J. G.: A new sea ice albedo scheme including melt ponds for ECHAM5 general circulation model, J. Geophys. Res., 114, D08101, doi:10.1029/2008JD010440, 2009. 1725
Pringle, D. J., Eicken, H., Trodahl, H. J., and Backstrom, L. G. E.: Thermal conductivity of landfast Antarctic and Arctic sea ice, J. Geophys. Res., 112, C04017, doi:10.1029/2006JC003641, 2007. 1747
Rees Jones, D. W. and Worster, M. G.: Fluxes through steady chimneys in a mushy layer during binary alloy solidification, J. Fluid Mech., 714, 127–151, 2013. 1725

TCD
8, 1723–1793, 2014

Saenz, B. T. and Arrigo, K. R.: Simulation of a sea ice ecosystem using a hybrid model for slush layer desalination, J. Geophys. Res., 117, C05007, doi:10.1029/2011JC007544, 2012. 1725
Schwarzacher, W.: Pack-ice studies in the Arctic Ocean, J. Geophys. Res., 64, 2357–2367, 1959. 1757, 1758, 1767, 1769, 1787, 1790
Tedesco, L., Vichi, M., Haapala, J., and Stipa, T.: A dynamic biologically active layer for numerical studies of the sea ice ecosystem, Ocean Model., 35, 89–104, 2010. 1725
Tedesco, L., Vichi, M., and Thomas, D. N.: Process studies on the ecological coupling between sea ice algae and phytoplankton, Ecol. Model., 226, 120–138, 2012. 1725
Turner, A. K., Hunke, E. C., and Bitz, C. M.: Two modes of sea-ice gravity drainage: a parameterization for large-scale modeling, J. Geophys. Res., 118, 2279–2294, 2013. 1725, 1726
Vancoppenolle, M., Fichefet, T., and Bitz, C. M.: Modeling the salinity profile of undeformed Arctic sea ice, Geophys. Res. Lett., 33, L21501, doi:10.1029/2006GL028342, 2006. 1725, 1736, 1737
Vancoppenolle, M., Bitz, C. M., and Fichefet, T.: Summer landfast sea ice desalination at Point Barrow, Alaska: modeling and observations, J. Geophys. Res., 112, C04022, doi:10.1029/2006JC003493, 2007. 1725, 1726, 1737, 1766
Vancoppenolle, M., Fichefet, T., Goosse, H., Bouillon, S., Madec, G., and Maqueda, M. A. M.: Simulating the mass balance and salinity of Arctic and Antarctic sea ice. 1. Model description and validation, Ocean Model., 27, 33–53, doi:10.1016/j.ocemod.2008.10.005, 2009. 1725, 1726, 1763, 1766, 1769
Vancoppenolle, M., Goosse, H., de Montety, A., Fichefet, T., Tremblay, B., and Tison, J.-L.: Modeling brine and nutrient dynamics in Antarctic sea ice: the case of dissolved silica, J. Geophys. Res., 115, C02005, doi:10.1029/2009JC005369, 2010. 1725
Vancoppenolle, M., Notz, D., Vivier, F., Tison, J., Delille, B., Carnat, G., Zhou, J., Jardon, F., Griewank, P., Lourenço, A., and Haskell, T.: Technical Note: On the use of the mushy-layer Rayleigh number for the interpretation of sea-ice-core data, The Cryosphere Discuss., 7, 3209–3230, doi:10.5194/tcd-7-3209-2013, 2013. 1729
Weeks, W. F. and Lee, O. S.: Observations on the physical properties of sea-ice at Hopedale, Labrador, Arctic, 11, 134–155, 1958. 1752
Wells, A. J., Wettlaufer, J. S., and Orszag, S. A.: Brine fluxes from growing sea ice, Geophys. Res. Lett., 38, L04501, doi:10.1029/2010GL046288, 2011. 1725

TCD
8, 1723–1793, 2014

Wettlaufer, J. S., Worster, M. G., and Huppert, H. E.: Natural convection during solidification of an alloy from above with application to the evolution of sea ice, J. Fluid Mech., 344, 291–316, doi:10.1017/S0022112097006022, 1997. 1759

Widell, K., Fer, I., and Haugan, P. M.: Salt release from warming sea ice, Geophys. Res. Lett., 33, L12501, doi:10.1029/2006GL026262, 2006. 1760

Wiese, M.: Laboratory experiments on the thermodynamics of melting sea ice, M.S. thesis, Meteorologisches Institut, Department Geowissenschaften, University Hamburg, 2012. 1747

TCD
8, 1723–1793, 2014

Table 1. Default model settings and free parameter values of salinity parametrizations.

Δz_0	1 cm
dt	10 s
N_{top}	20
N_{mid}	60
N_{bot}	20
$\phi_{\text{s, min}}$	0.05
$\phi_{\text{s, melt}}$	0.4
$\phi_{\text{g, melt}}$	0.2
alb	0.75
pen	0.3
κ	$2\,\text{m}^{-1}$
α	$5.84 \times 10^{-4}\,\text{kg m}^{-3}\,\text{s}^{-1}$
R_{crit}	4.89
γ	0.99
β	1
δ	0.5
ϵ	0.1
ζ_{max}	5 cm

TCD
8, 1723–1793, 2014

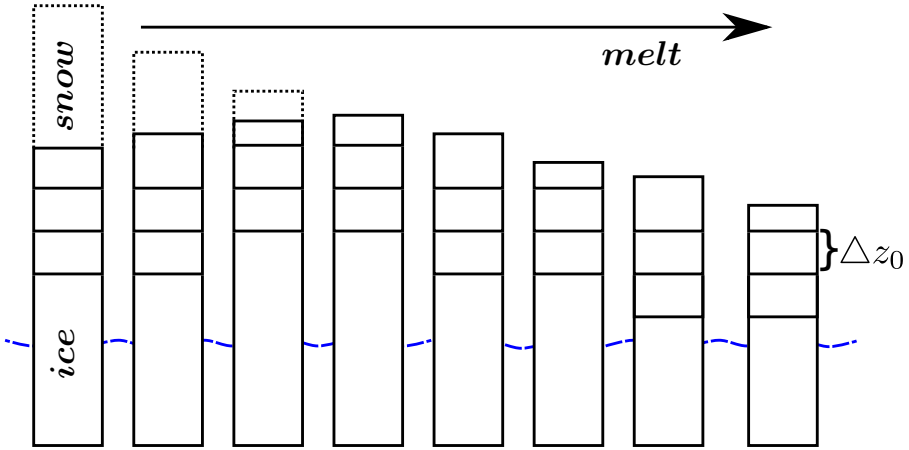

Fig. 1. Sketch of SAMSIM grid evolution for three top ice layers during snow melt and following surface ablation as explained in Sect. 2.3.

TCD
8, 1723–1793, 2014

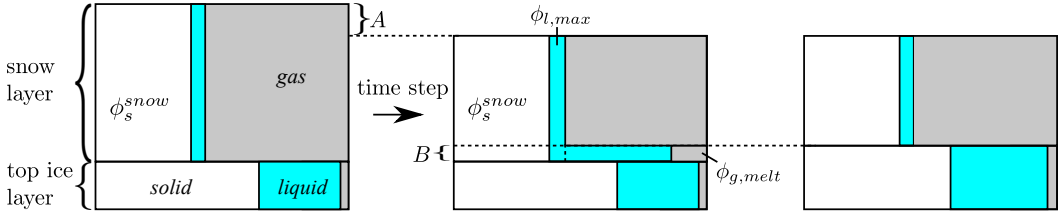

Fig. 2. Sketch of snow melt by snow to slush conversion as described in Sect. 2.3.1. B is the thickness of the slush layer, and A is the thickness lost by snow to slush conversion. At the end of the time step the top ice layer thickness increases by B while the snow layer thickness is reduced by $A + B$. The white, blue, and grey areas represent the solid, liquid, and gas volume fractions of each model layer.

TCD
8, 1723–1793, 2014

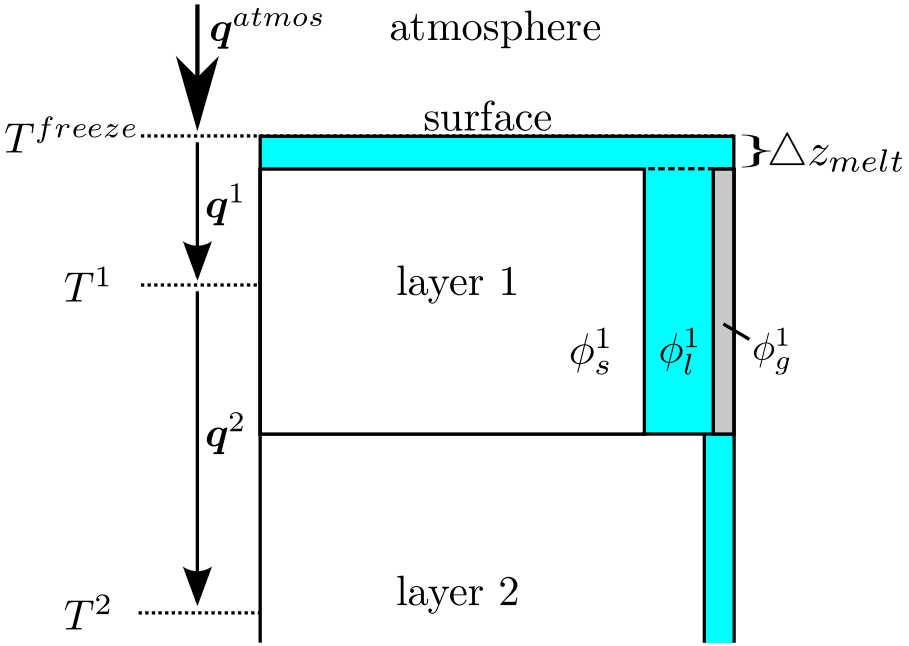

Fig. 3. Sketch of melt water formation caused by surface melting as described in Sect. 2.3.2. The white, blue, and grey areas represent the solid, liquid, and gas volume fractions of each model layer (ϕ_s, ϕ_l, and ϕ_g). Δz_{melt} is determined by the amount of latent heat release necessary to balance the energy difference between the atmospheric heat flux to the surface $\boldsymbol{q}^{atmos}$ and the flux from the surface into the top ice layer $\boldsymbol{q}^1$.

TCD
8, 1723–1793, 2014

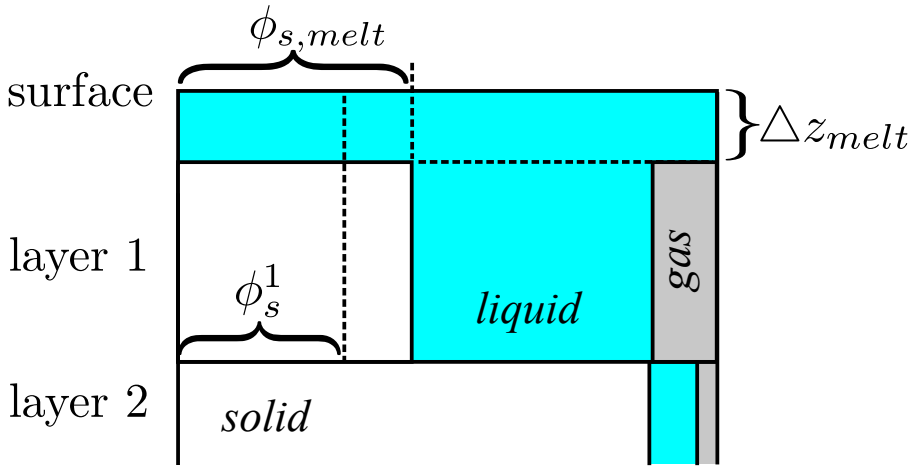

Fig. 4. Formation of melt water in the top ice layer when $\phi_s^1 < \phi_{s,melt}$ as described in Sect. 2.3.2. Δz_{melt} is determined by how much the solid fraction has to be raised to equal $\phi_{s,melt}$. The white, blue, and grey areas represent the solid, liquid, and gas volume fractions of each model layer.

TCD
8, 1723–1793, 2014

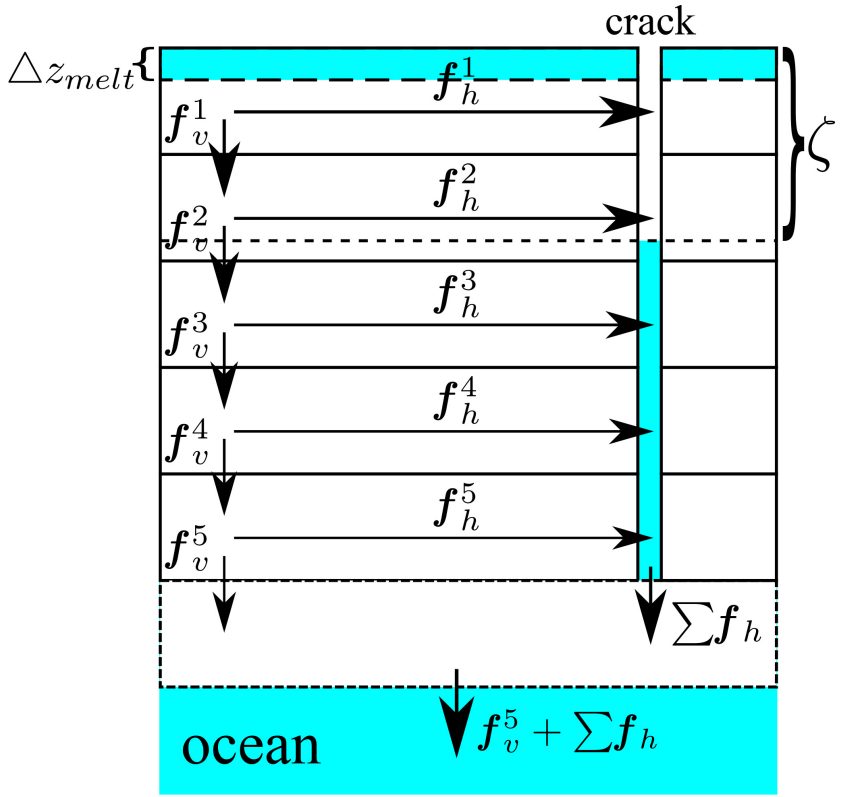

Fig. 5. Brine fluxes of the complex flushing parametrization resulting from melt water formation at the surface as described in Sect. 2.4.2. The horizontal fluxes $\boldsymbol{f}_h$ transport heat and salt to the lowest layer directly via cracks in the ice, while the vertical fluxes $\boldsymbol{f}_v$ advect heat and salt from layer to layer. ζ is the freeboard of the ice and Δz_{melt} is the depth of the melt water.

TCD
8, 1723–1793, 2014

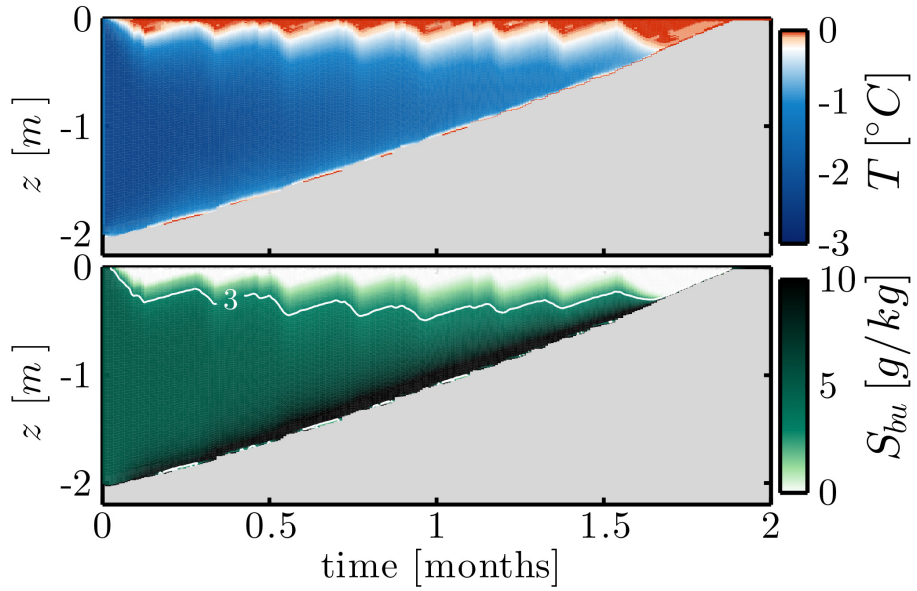

Fig. 6. Temperature **(a)** and bulk salinity **(b)** evolution of the idealized flushing experiment using the default model setup (experiment setup in Sect. 3, model setup in Table 1). Temperature color bar is white at the freezing temperature of the initial ice salinity of 5 g kg^{-1}. Plot background is grey.

TCD
8, 1723–1793, 2014

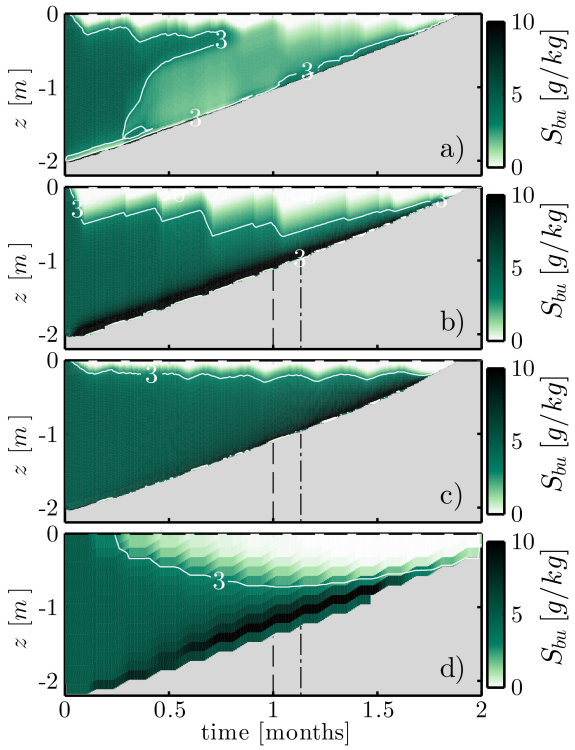

Fig. 7. Salinity evolution of the idealized melting experiments in which one specific parameter or setting has been changed from the default values (default model results shown in Fig. 6, experiment description can be found in Sect. 3, default settings are listed in Table 1). The white line is the 3 g kg^{-1} salinity contour. **(a)** includes gravity drainage which is otherwise disabled in the experiment. In **(b)** the minimal solid fraction of the top ice layer $\phi_{s,\,melt}$ is 0.2 instead of 0.4. In **(c)** the ratio of horizontal to vertical hydraulic resistance β is 0.2 instead of 1.0. In **(d)** the vertical spatial resolution Δz_0 is 12.8 cm instead of 1 cm. The dashed black lines in **(b–d)** mark the times at which the profiles in Fig. 8 are shown.

TCD
8, 1723–1793, 2014

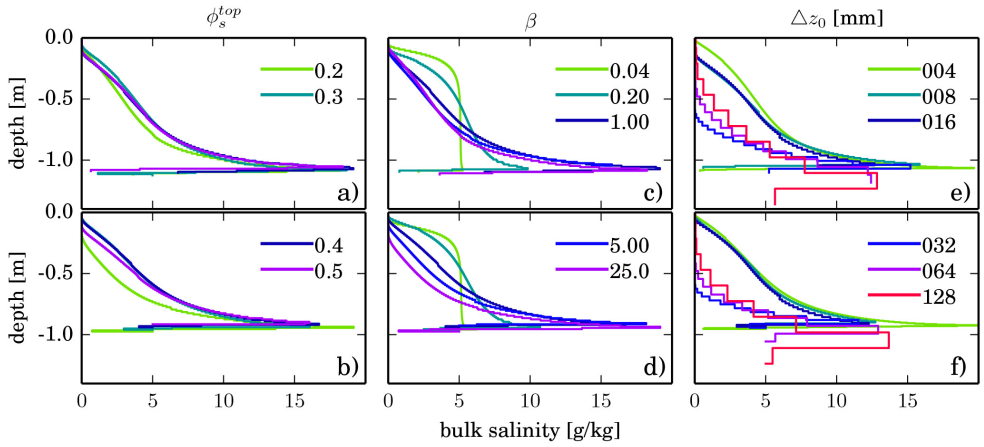

Fig. 8. Salinity profiles of the idealized melting experiments after 30 days **(a, c, e)** and after 34 days **(b, d, f)**. Profiles are shown at two separate times to visualize the short-term variations due to oscillations. The experiment description can be found in Sect. 3 and the point of time of the profiles are marked in Fig. 7 by dashed lines. In **(a, b)** the minimal solid fraction of the top ice layer $\phi_{s,\,melt}$ is varied (see Sect. 3.2), in **(c, d)** the ratio of horizontal to vertical hydraulic resistance β is varied (see Sect. 3.3), and in **(e, f)** the vertical spatial resolution Δz_0 is changed (see Sect. 3.4). The subfigures above and below each other share their legend (e.g. **a** and **b**).

TCD
8, 1723–1793, 2014

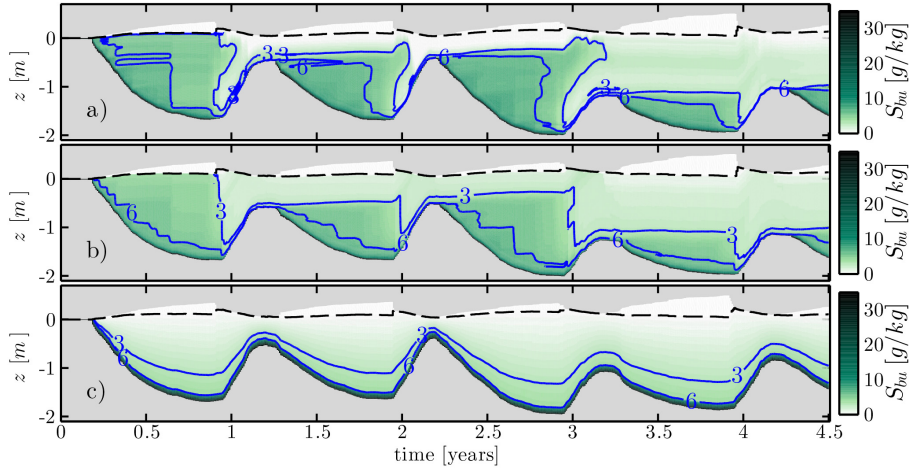

Fig. 9. Salinity evolution of the **(a)** complex, **(b)** simple, and **(c)** prescribed salinity approach for one of the nine Arctic simulations forced with ERA-interim data from 75° N and 145° W. The salinity approaches are described in Sect. 2.5, and the model setup is described in Sect. 4.1. The simulation time (x axis) begins on 1 July 2005. The dashed line marks the snow-ice boundary. The water surface is at $z = 0$.

TCD
8, 1723–1793, 2014

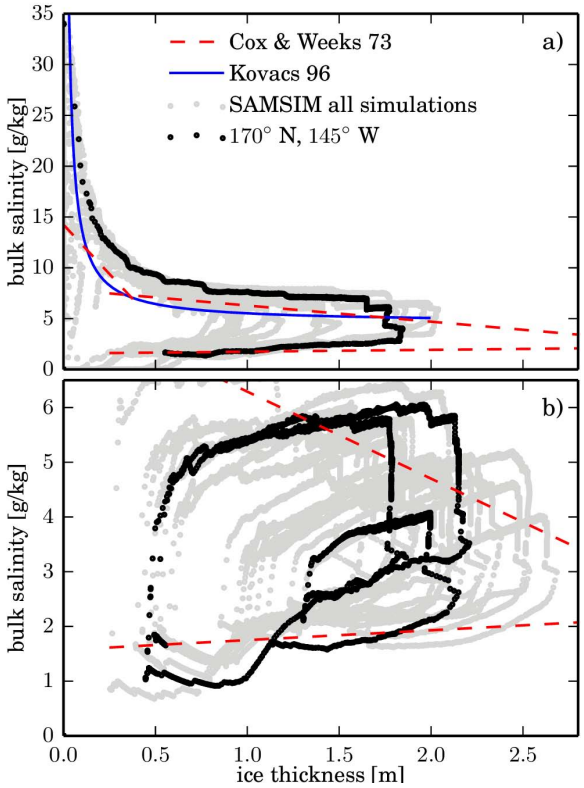

Fig. 10. The vertically integrated vertical bulk salinity as a function of ice thickness for all reanalysis forced runs as described in Sect. 4.1. Each grey dot represents a 12 hourly snapshot. **(a)** contains all 15 years of first-year ice and **(b)** contains all 21 years of multi-year ice in grey. Of all nine simulations a single simulation is plotted in black (80° N, 90° E) to enable tracking the evolution over time. The blue curve in **(a)** is the empirical relationship for first-year ice published by Kovacs (1997) for ice up to 2 m. The red dashed lines mark the empirical linear relationships found by Cox and Weeks (1974) for growing (upper lines) and melting Arctic ice (lower line).

TCD
8, 1723–1793, 2014

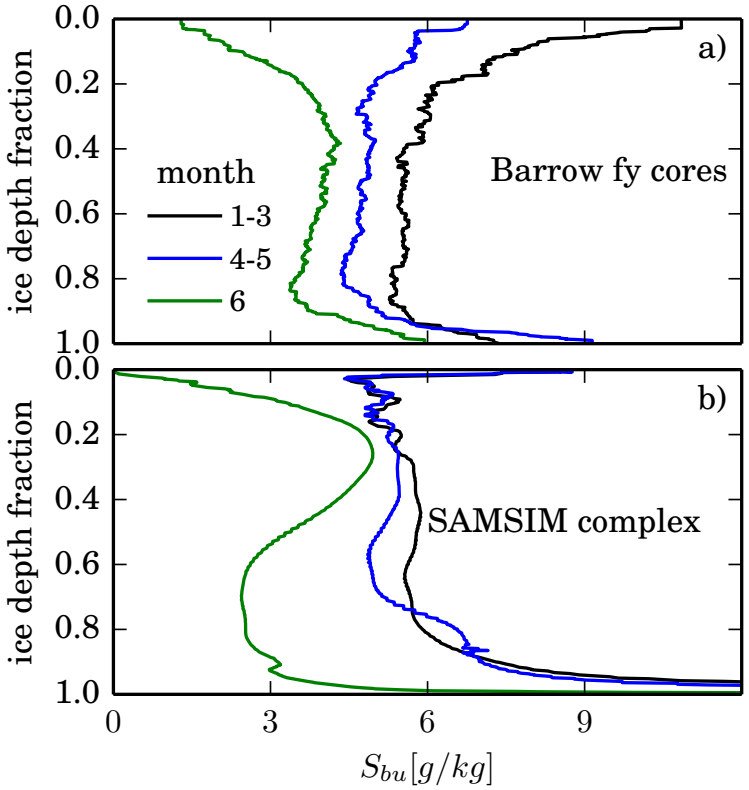

Fig. 11. Time-averaged and vertically-normalized salinity profiles from first-year ice cores (described in Sect. 4.3 and shown in **a**) and first year ice from reanalysis forced simulations using the complex brine dynamic parametrizations **(b)**. Both were averaged from January to March (1–3), April to May (4–5), and over June (6).

TCD
8, 1723–1793, 2014

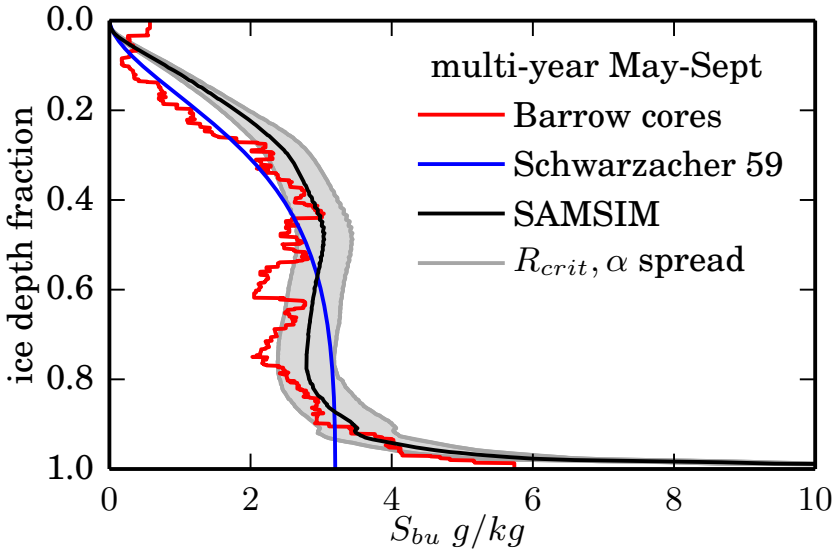

Fig. 12. May to September mean of vertically-normalized multi-year salinity profiles of reanalysis forced simulations using the complex brine dynamic parametrizations. Schwarzacher 59 refers to the fitted profile of Schwarzacher (1959), and Barrow cores refers to the multi-year ice cores taken by the Alaska Ocean Observing System from 1999–2011 (Eicken et al., 2012). The R_{crit}, α spread shows the SAMSIM profile using the two non-default values of the gravity drainage parameters obtained from the optimization process (see Sect. 2.2). Left line: $\alpha = 0.000681, R_{\text{crit}} = 3.23$. Right line: $\alpha = 0.000510, R_{\text{crit}} = 7.10$. The area between the two simulations is shaded in light grey.

TCD
8, 1723–1793, 2014

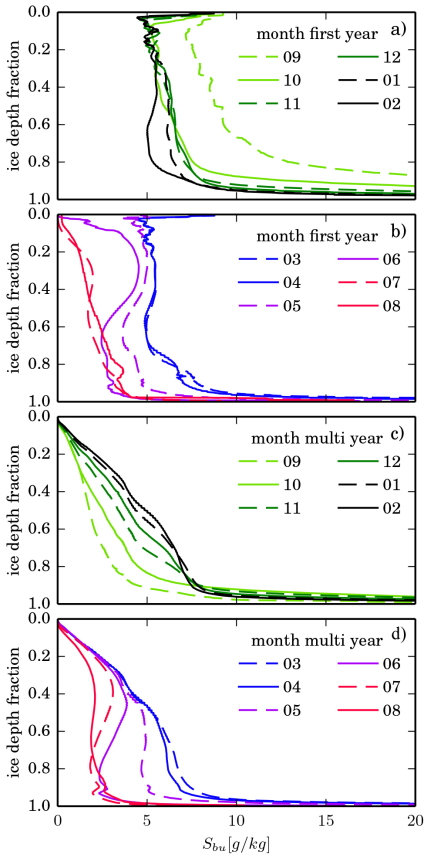

Fig. 13. Monthly mean of vertically-normalized salinity profiles of reanalysis forced simulations using the complex brine dynamic parametrizations as described in Sect. 4.1. The simulations were split into annual cycles beginning in September (month 9) and sorted into 15 years of first-year ice (**a** and **b**) and 21 years of multi-year ice (**c** and **d**). The corresponding ice thickness of the monthly means are shown in Fig. 14.

TCD
8, 1723–1793, 2014

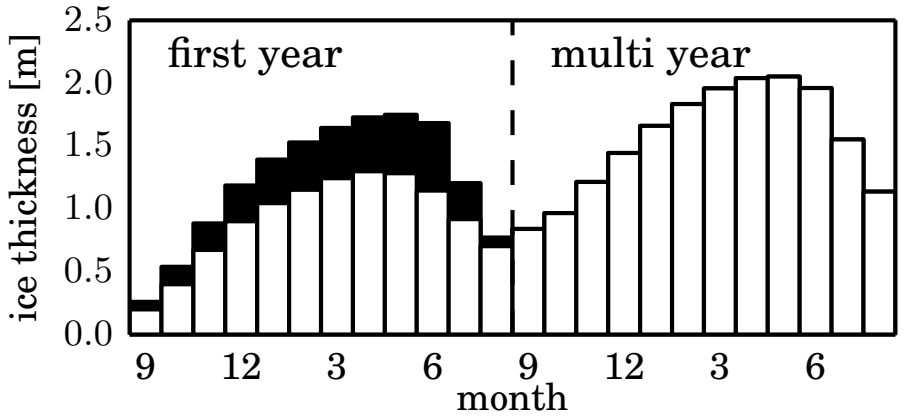

Fig. 14. The white columns show the thickness of all monthly mean salinity profiles shown in Fig. 13. The black columns represent only first-year ice which evolves into multi-year ice the following year. To be included in the monthly average ice must be present, meaning that model output of ice-free water with an ice thickness of zero is excluded from the mean.

TCD
8, 1723–1793, 2014

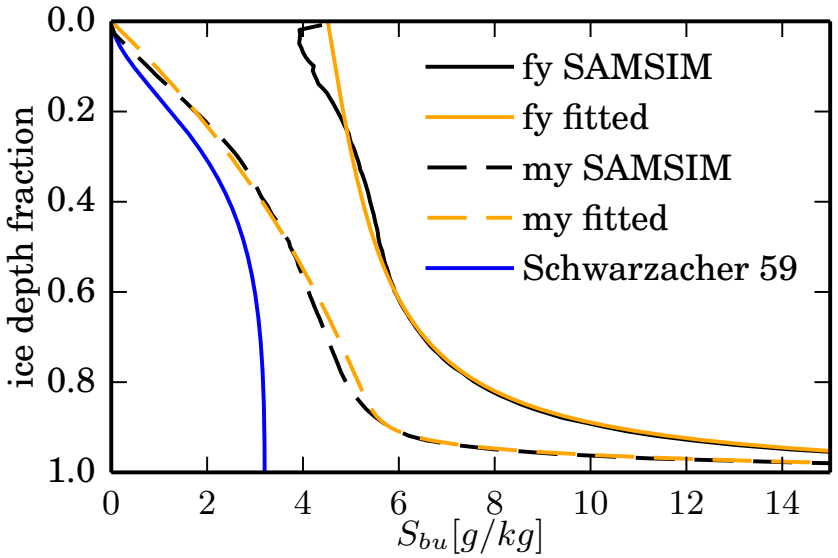

Fig. 15. Yearly mean first-year (fy) and multi-year (my) sea-ice salinity profiles of SAMSIM using the complex parametrization. The fitted analytical functions of the profiles listed in Sect. 4.4 are added in orange. Although the profile of Schwarzacher (1959) is summer biased (see Sect. 4.3.3), we have included it as a reference.

TCD
8, 1723–1793, 2014

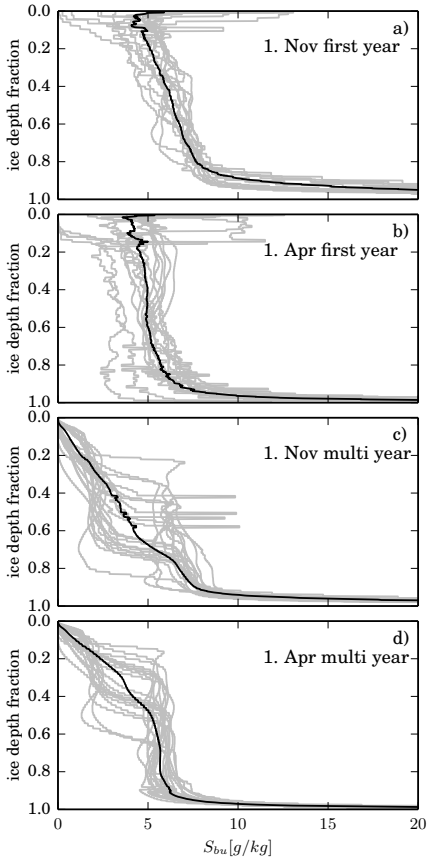

Fig. 16. Vertically-normalized salinity profiles of the reanalysis forced simulations (described in Sect. 4.1) using the complex salinity parametrizations at the first of November (**a** and **c**) and the first of April (**b** and **d**). First-year ice (**a** and **b**) and multi-year ice (**c** and **d**) are shown separately. The grey lines are the individual model realizations and the black line is the average over all profiles.

TCD
8, 1723–1793, 2014

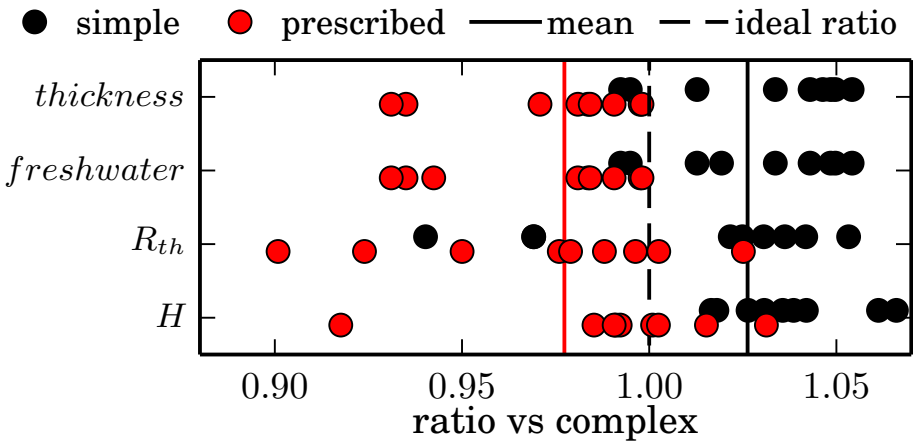

Fig. 17. Ratios of the time integrated ice thickness, freshwater column, thermal resistance R_{th}, and enthalpy H of the simple and the prescribed SAMSIM salinity approach compared against the complex approach (details in Sect. 5). The ratios were calculated separately for each of the nine reanalysis forced simulations over 4.5 years. Each dot shows the ratio of a specific simulation, while the lines show the mean over all runs and quantities.

TCD
8, 1723–1793, 2014

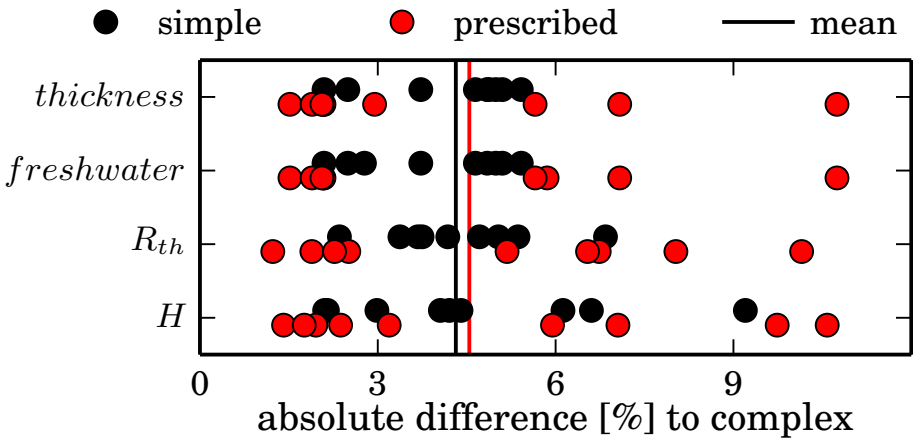

Fig. 18. Time integrated absolute differences of the ice thickness, freshwater column, thermal resistance R_{th}, and enthalpy H of simulations using the simple and prescribed SAMSIM salinity approach compared against simulations using the complex approach (details in Sect. 5). The absolute differences were calculated separately for each of the nine reanalysis forced simulations over 4.5 years. Each dot shows the ratio of a specific simulation, while the lines show the mean over all runs and quantities.

TCD
8, 1723–1793, 2014